J Intell Robot Syst (2018) 89:191–210
DOI 10.1007/s10846-017-0482-0

VFO Path following Control with Guarantees of Positionally Constrained Transients for Unicycle-Like Robots with Constrained Control Input

Maciej Marcin Michałek · **Tomasz Gawron**

Received: 8 March 2016 / Accepted: 15 January 2017 / Published online: 27 January 2017

Abstract The Vector-Field-Orientation (VFO) method is a control design concept which was originally introduced for the unicycle kinematics to solve two classical control tasks corresponding to the trajectory tracking and set-point control problems. A unified solution to both the tasks was possible by appropriate definitions of the so-called convergence vector field. So far, there has not been a version of the VFO control law for the third classical control task concerning the path following problem, which is particularly meaningful in the context of practical applications. The paper fills this gap by presenting a novel VFO path following controller devised for robots of unicycle-like kinematics with the amplitude-limited control input. Opposite to most path following controllers proposed in the literature, the new control law utilizes the recently introduced *level curve* approach which does not employ any parametrization of a reference path. In this way, the proposed solution is free of main limitations resulting from the need of unique determination of the shortest distance from a robot to the path. In contrast to other solutions, a formal analysis of the closed-loop dynamics presented in this paper provides sufficient conditions which guarantee constrained transients of robot motion with the position confined to a prescribed subset around a reference path. Theoretical results have been validated by numerical examples and experimentally verified with utilization of a laboratory-scale differentially driven robot.

Keywords Path following · Unicycle · Control input constraints · State constraints · Level-curve approach · VFO

1 Introduction

The path following (PF) problem belongs to the collection of classical control tasks defined for mobile robots [6]. Unlike in the trajectory tracking problem, the PF task does not impose time constraints on the robot motion apart from a geometry determined by a reference path. Numerous solutions to the PF problem have been proposed in the literature with applications to various structures of robotic vehicles [1, 2, 7, 16–19, 28, 29], in particular to the nonholonomic wheeled robots of unicycle-like kinematics [6, 12–14, 25, 27]. Essential geometry of planar motion for any single-body nonholonomic vehicle can be generically

This work was financially supported by the National Science Centre, Poland, as the research grant No. 2016/21/B/ST7/02259.

M. M. Michałek (✉) · T. Gawron
Chair of Control and Systems Engineering,
Poznan University of Technology (PUT),
Piotrowo 3A, 60-965 Poznań, Poland
e-mail: maciej.michalek@put.poznan.pl

T. Gawron
e-mail: tomasz.gawron@doctorate.put.poznan.pl

described by a unicycle kinematic model. As a consequence, applicability of control laws devised for the unicycle model can be relatively easily extended to more complex kinematics by employing the cascade-like control approach – see, e.g., [20, 22, 23].

All the available control laws solving the PF problem can be divided into two general groups: those employing some parametrization of a reference path (usually by using an arc-length parametrization), and these not using any path parametrization but instead applying the so-called level curve approach. The first group originates from the classical concept [29], where the parametrization combined with a projection (orthogonal [29] or non-orthogonal [15]) of a current robot position on the path allow one to uniquely select the *current point* on a reference path in correspondence to which all the path following errors may be determined. Successful application of this approach in the most popular version with the orthogonal projection requires determination of the shortest distance to a path, which is generally a nontrivial issue and is valid only locally in a sufficiently small neighborhood of a reference path. Locality, in turn, imposes conservative limitations on the initial robot position with respect to the path.

Algorithms from the second group employ a completely different idea, where a reference path is defined implicitly as a set of reference points satisfying some scalar equation. Evaluating this equation for the points taken from the reference set gives the zero value, while for the points outside the reference set – a non-zero value. This non-zero value is treated as a signed measure of a robot distance to the reference set. In this way, the need of computations of the shortest distance to a path is avoided. Simplicity of practical implementation of the control laws applying the level curve approach makes them particularly attractive for the robotics community. However, to the authors' best knowledge, so far only few controllers have been proposed and applied to robotic vehicles using this concept. It has been utilized in [5] in the context of the VTOL aerial vehicles, while its application to the unicycle-like wheeled robot has been presented in [26] (see also [30]) on a kinematic level, and in [8] considering both kinematics and dynamics of a vehicle. Worth to mention also works [4] and [20] presenting applications of the level curve approach to the coordinated multiple unicycles and to the N-trailer robots, respectively.

This paper presents a novel solution to the PF problem for unicycle-like kinematics formulated in the VFO (*Vector Field Orientation*, [9]) framework and utilizing the level curve approach for definition of a reference set. The main contribution of this work relies on an introduction of a newly devised version of the VFO control law specialized to the (positionally constrained) PF problem, not addressed so far in any of the previous works devoted to the VFO control method. The proposed solution can be applied to a wider class of reference paths than those admitted in [8], and guarantees the absence of any unstable closed-loop equilibria in contrast to the method presented in [26]. Formal stability guarantees provided in the paper explicitly take into account control input limitations imposed on a robot (not addressed in [26]). Moreover, we determine sufficient conditions guaranteeing that position of a robot remains in a prescribed neighborhood of a reference path during the whole transient stage of the control process. This utility, not considered by the authors of works [26] and [8], may have an essential practical meaning for motion control applications in the cluttered environments. Finally, the new proposition complements a family of the VFO control laws, introduced so far for the tracking task and the stabilization problem, see [9, 21].

Notation For the sake of concise notation, we will apply a short notation $\mathrm{s}\alpha \equiv \sin\alpha$, $\mathrm{c}\alpha \equiv \cos\alpha$ in the whole text. By symbol $\|\cdot\|$ we will denote the standard Euclidean norm.

2 Prerequisites and Problem Formulation

2.1 Vehicle Model and Control Input Constraints

Let us consider the unicycle-like mobile robot presented in Fig. 1 which can be described by kinematics

$$\dot{\boldsymbol{q}}(t) = \begin{bmatrix} 1 & 0 \\ 0 & \mathrm{c}\theta(t) \\ 0 & \mathrm{s}\theta(t) \end{bmatrix} \boldsymbol{u}(t) = \begin{bmatrix} \boldsymbol{g}_1 & \boldsymbol{g}_2(\theta(t)) \end{bmatrix} \begin{bmatrix} u_1(t) \\ u_2(t) \end{bmatrix} \tag{1}$$

where

$$\boldsymbol{q} = [\theta \; x \;\; y]^\top = \begin{bmatrix} \theta \\ \boldsymbol{p} \end{bmatrix} \in \mathbb{R}^3 \tag{2}$$

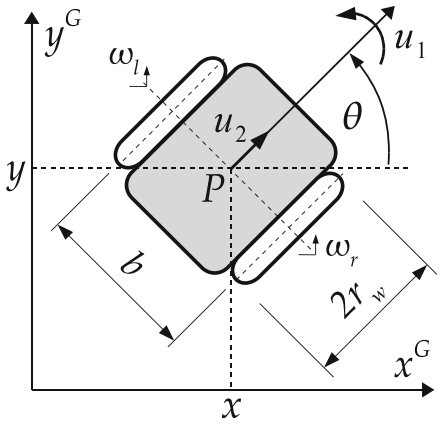

Fig. 1 A unicycle-like mobile robot in a global frame $\{x^G, y^G\}$

defines the vehicle configuration, while $\boldsymbol{u} = [u_1\ u_2]^\top \in \mathcal{U} \subset \mathbb{R}^2$ is a control input comprising the angular velocity u_1 of a vehicle body and the longitudinal velocity u_2 of the so-called *guidance point* P.

In the field of wheeled mobile robots, kinematics (1) usually corresponds to the differentially-driven locomotion where the two wheels of the robot from Fig. 1 are independently driven by two actuators. A relation joining robot-body (pseudo) velocities in vector $\boldsymbol{u}$ with angular velocities $\boldsymbol{\Omega} = [\omega_r\ \omega_l]^\top$ of the robot right and left wheels, respectively, comes from the well-known equation

$$\boldsymbol{\Omega} = \begin{bmatrix} \omega_r \\ \omega_l \end{bmatrix} = \boldsymbol{J}^{-1}\boldsymbol{u}, \qquad \boldsymbol{J} = \begin{bmatrix} r_w/b & -r_w/b \\ r_w/2 & r_w/2 \end{bmatrix}, \tag{3}$$

where $r_w > 0$ and $b > 0$ denote the wheel radius and the wheels base, respectively, shown in Fig. 1.

From now on, we will assume that control input $\boldsymbol{u} \in \mathcal{U}$ is subject to constraints resulting from a prescribed maximal admissible angular velocity $\omega_m > 0$ of a robot wheel. As a consequence, we postulate that angular velocities of the robot wheels should satisfy

$$\forall\, t \geq 0\ \ |\omega_r(t)| \leq \omega_m\ \ \wedge\ \ |\omega_l(t)| \leq \omega_m. \tag{4}$$

Condition (4) implicitly (by the inverse relation to Eq. 3) imposes (interdependent) constraints on the control inputs u_1 and u_2, [21].

2.2 Definition of a Reference Path

Define a subset $\mathcal{D} \subset \mathbb{R}^2$ of positions $\boldsymbol{p} = [x\ y]^\top$, and a positional reference path as a set $S_d \subset \mathcal{D}$ of points $\boldsymbol{p}_d = [x_d\ y_d]^\top$ such that

$$S_d \triangleq \{\boldsymbol{p}_d \in \mathcal{D}:\ F(\boldsymbol{p}_d) \triangleq \sigma f(\boldsymbol{p}_d) = 0\}, \tag{5}$$

where the coefficient $\sigma \in \mathbb{R} \setminus \{0\}$ and an analytical form of the scalar function $f(\boldsymbol{p}_d)$ are the design terms. In contrast to the classical parametrized form, a reference path has been implicitly defined by Eq. 5 as a zero-level curve of some function $F : \mathbb{R}^2 \to \mathbb{R}$ such that $F(\boldsymbol{p}) = 0 \ \Leftrightarrow\ \boldsymbol{p} \in S_d$, and $F(\boldsymbol{p}) = c \neq 0$ if $\boldsymbol{p} \notin S_d$. The sign of coefficient σ in Eq. 5 will determine a desired motion direction along a reference path in a global frame, that is, either the clockwise/counter-clockwise or the right/left direction (see definition (7)).

For the reference set (5) we assume what follows.

A1. For any bounded $\boldsymbol{p} = [x\ y]^\top \in \mathcal{D}$ the function $F(\boldsymbol{p})$ takes values from a bounded subset $\mathcal{D}_F \triangleq [\underline{F}, \overline{F}] \subset \mathbb{R}$, $\underline{F} \in (-\infty, 0)$, $\overline{F} \in (0, \infty)$; furthermore, function $F(\boldsymbol{p})$ for $\boldsymbol{p} \in \mathcal{D}$ is at least twice differentiable with respect to its arguments, that is, there exist bounded partial derivatives

$$F_x(\boldsymbol{p}) \triangleq \frac{\partial F}{\partial x}, \quad F_y(\boldsymbol{p}) \triangleq \frac{\partial F}{\partial y}, \quad F_{z_1 z_2}(\boldsymbol{p}) \triangleq \frac{\partial^2 F}{\partial z_1 \partial z_2}$$

for $z_1, z_2 \in \{x, y\}$.

A2. $\|\nabla F(p)\| \triangleq \sqrt{F_x^2(\boldsymbol{p}) + F_y^2(\boldsymbol{p})} \in [\underline{m}, \overline{m}]$ for all $p \in \mathcal{D}$, where $0 < \underline{m} \leq \overline{m} < \infty$ are the lower and upper bounds of the function gradient norm, respectively.

A3. A reference longitudinal velocity along a reference path is restricted to the form

$$u_{2d} \triangleq \zeta_d v_d, \quad v_d = \text{const} > 0, \quad \zeta_d \in \{-1, +1\}, \tag{6}$$

where ζ_d determines a desired motion strategy along a reference path, i.e., forward motion for $\zeta_d := +1$ or backward motion for $\zeta_d := -1$. Note that a definition of a non-constant velocity u_{2d} would require some parametrization of u_{2d} along a reference path. Since the level curve approach avoids parametrization of

a path, we restrict further considerations to the case proposed in Eq. 6.

Reference orientations tangent to the reference path determined by set (5) will be defined as

$$\theta_d(\boldsymbol{p}_d) \triangleq \mathrm{Atan2}\left(\zeta_d F_x(\boldsymbol{p}_d)\,,\, -\zeta_d F_y(\boldsymbol{p}_d)\right) \in [-\pi, \pi), \tag{7}$$

where $\mathrm{Atan2}(\cdot,\cdot) : \mathbb{R}\times\mathbb{R} \to [-\pi,\pi)$ is a four-quadrant inverse tangent function. Note that the signs of coefficients σ used in definition (5) and ζ_d introduced in Eq. 6 both determine the resultant quadrants in which the reference angle (7) is defined.

Remark 1 One assumes that the upper bound ω_m introduced in Eq. 4 is large enough to ensure that a reference path can be perfectly followed with the reference longitudinal velocity (6) without velocity saturation of any of the robot wheels. That is, one assumes that for all $t \geq 0$ holds

$$|\omega_{rd}(t)|\,,\, |\omega_{ld}(t)| < \omega_m \;\text{ where }\; \begin{bmatrix} \omega_{rd} \\ \omega_{ld} \end{bmatrix} = \boldsymbol{J}^{-1} \begin{bmatrix} \dot{\theta}_d \\ u_{2d} \end{bmatrix}. \tag{8}$$

All the subsequent considerations implicitly assume satisfaction of inequality (8).

2.3 Control Problem Formulation

Following the idea suggested in [30], we will treat $F(\boldsymbol{p})$ as a positional measure of the path following error. It seems justified because $F(\boldsymbol{p})$ is zero if and only if $\boldsymbol{p} \in S_d$, while a sign of a value of $F(\boldsymbol{p})$ for $\boldsymbol{p} \notin S_d$ depends on a side on which the robot position stays relative to the reference path.[1] Let us define the path following error as follows

$$\boldsymbol{e}(\boldsymbol{q}) = \begin{bmatrix} e_\theta(\theta) \\ e_F(\boldsymbol{p}) \end{bmatrix} \triangleq \begin{bmatrix} \rho(\theta_d(\boldsymbol{p}) - \theta) \\ F(\boldsymbol{p}) \end{bmatrix} \in [-\pi,\pi)\times\mathbb{R}, \tag{9}$$

where function $\rho : \mathbb{R} \to [-\pi,\pi)$ confines the orientation error to the range $[-\pi,\pi)$, while the form of $\theta_d(\boldsymbol{p})$ results from Eq. 7.

[1] Note, however, that in general a value of $|F(\boldsymbol{p})|$ does not correspond to the Euclidean distance from a robot to a reference path.

Definition 1 (**Positionally Constrained PF Problem**) The objective is to find a bounded feedback control law $\boldsymbol{u} = \boldsymbol{u}(\boldsymbol{q})$ for kinematics (1) satisfying velocity limitations (4), which guarantees boundedness and asymptotic convergence of error (9) in the sense

$$\forall\, t \geq 0 \;\; \boldsymbol{e}(\boldsymbol{q}(t)) \in [-\pi,\pi)\times\mathcal{D}_F^* \quad \wedge \quad \boldsymbol{e}(\boldsymbol{q}(t)) \overset{t\to\infty}{\longrightarrow} \boldsymbol{0}. \tag{10}$$

where $\mathcal{D}_F^* \subset \mathcal{D}_F \subset \mathbb{R}$ is some prescribed positional subset.

In contrast to the conventional PF problem, Definition 1 imposes a requirement of a positionally constrained robot motion determined by the prescribed subset $\mathcal{D}_F^*$. This functionality can be especially useful for control applications in the cluttered environments. In the next section, we will propose a solution to the above stated problem employing the VFO approach.

3 The VFO Control Law for the PF Problem

3.1 General Form of the VFO Control Law

A general structure of the VFO control law for unicycle kinematics (1) can be derived upon the Vector Field Orientation methodology presented in [9]. According to this methodology, one postulates the existence of the so-called *convergence vector field*

$$\boldsymbol{h}(\boldsymbol{q},\cdot) = \begin{bmatrix} h_\theta(\boldsymbol{q},\cdot) \\ h_x(\boldsymbol{q},\cdot) \\ h_y(\boldsymbol{q},\cdot) \end{bmatrix} = \begin{bmatrix} h_\theta(\boldsymbol{q},\cdot) \\ \overline{\boldsymbol{h}}(\boldsymbol{q},\cdot) \end{bmatrix} \in \mathbb{R}\times\mathbb{R}^2, \tag{11}$$

which has a meaning of a generalized velocity with angular component h_θ and longitudinal component $\overline{\boldsymbol{h}} = [h_x\; h_y]^\top$. For every configuration $\boldsymbol{q}$ the convergence vector field determines an instantaneous desirable direction of motion and orientation for a robot to reach the goal, which can be represented by a reference point, a reference trajectory, or (as in the current case) a reference path. Particular forms of vector field (11) have to be independently defined for particular control problems; they determine a desirable transient behavior and steady motion for a robot. In the VFO methodology, one aims to find a control law which

guarantees tracking of the convergence vector field by the configuration velocity of the unicycle. It can be expressed by the postulate $\dot{\boldsymbol{q}}(t) = \boldsymbol{h}(\boldsymbol{q}(t), \cdot)$. By substituting for $\dot{\boldsymbol{q}}$ the particular terms from the right-hand side of Eq. 1, the formula $\dot{\boldsymbol{q}}(t) = \boldsymbol{h}(\boldsymbol{q}(t), \cdot)$ gives three postulated scalar equations, namely $u_1 = h_\theta$, $u_2 \mathrm{c}\theta = h_x$, and $u_2 \mathrm{s}\theta = h_y$. Multiplying the latter two equations by $\mathrm{c}\theta$ and $\mathrm{s}\theta$, respectively, and adding them by sides gives a postulated equation for the second control input in the form $u_2 = h_x \mathrm{c}\theta + h_y \mathrm{s}\theta$. Thus, a general form of the VFO control law can be written as follows (see [9]):

$$\boldsymbol{u}^{\mathrm{VFO}} = \begin{bmatrix} u_1^{\mathrm{VFO}} \\ u_2^{\mathrm{VFO}} \end{bmatrix} = \begin{bmatrix} h_\theta \\ h_x \mathrm{c}\theta + h_y \mathrm{s}\theta \end{bmatrix} \overset{(1)}{=} \begin{bmatrix} h_\theta \\ \boldsymbol{h}^\top \boldsymbol{g}_2(\theta) \end{bmatrix}. \tag{12}$$

The control components u_1^{VFO} and u_2^{VFO} have clear geometrical interpretation corresponding to a generalization of control in polar coordinates, according to which the former is called the *orienting control* while the latter is called the *pushing control* (for more details see [9]).

It is worth to emphasize that the general form of the VFO control (12) is valid regardless of the control problem under consideration, i.e., the point stabilization, the trajectory tracking, or the path following. The only difference comes from a definition of the convergence vector field (11) which must be specialized for a particular control task. So far, definitions of the vector field (11) have been proposed for two control tasks, i.e., for stabilization and tracking (see [3, 9]). In the next section, we will complement the available definitions with a new one specialized for the path following problem.

Hereafter, by saying about the *nominal* control applied into kinematics (1) we will understand the substitution

$$\boldsymbol{u} := \boldsymbol{u}_n \triangleq \boldsymbol{u}^{\mathrm{VFO}} \tag{13}$$

with $\boldsymbol{u}^{\mathrm{VFO}}$ defined by Eq. 12. By referring to the *nominal* control (indicated by the subscript n) we will understand the control conditions in which no control input constraints of the robot are taken into account. To address the control input constraints, we will apply the input scaling procedure presented in Section 3.3.

3.2 Definition of the Convergence Vector Field

We are going to define the convergence vector field (11) for the case of the PF Problem. To this aim, let us introduce two mutually orthogonal vectors

$$\boldsymbol{w}(\boldsymbol{p}) \triangleq -\nabla F(\boldsymbol{p}) = \begin{bmatrix} -F_x(\boldsymbol{p}) \\ -F_y(\boldsymbol{p}) \end{bmatrix} \in \mathbb{R}^2, \tag{14}$$

$$\boldsymbol{w}_\perp(\boldsymbol{p}) \triangleq \boldsymbol{R}\, \boldsymbol{w}(\boldsymbol{p}) \overset{(14)}{=} \begin{bmatrix} -F_y(\boldsymbol{p}) \\ F_x(\boldsymbol{p}) \end{bmatrix} \in \mathbb{R}^2, \tag{15}$$

where $\boldsymbol{R} = \left[\begin{smallmatrix} 0 & 1 \\ -1 & 0 \end{smallmatrix}\right]$ is a rotation matrix of angle $-\frac{\pi}{2}$, while F_x and F_y are the partial derivatives defined in assumption A1.

We propose to define a longitudinal component of the convergence vector field as follows

$$\begin{aligned} \overline{\boldsymbol{h}}(\boldsymbol{p}) = \begin{bmatrix} h_x(\boldsymbol{p}) \\ h_y(\boldsymbol{p}) \end{bmatrix} &\triangleq v_d \frac{\boldsymbol{w}_\perp(\boldsymbol{p})}{\|\nabla F(\boldsymbol{p})\|} + k_p F(\boldsymbol{p}) \frac{\boldsymbol{w}(\boldsymbol{p})}{\|\nabla F(\boldsymbol{p})\|} \\ &= \left(v_d \boldsymbol{R} + k_p F(\boldsymbol{p}) \boldsymbol{I}_{2\times 2}\right) \boldsymbol{\vartheta}(\boldsymbol{p}), \end{aligned} \tag{16}$$

where $\boldsymbol{I}_{2\times 2}$ is the identity matrix, $k_p > 0$ is a design parameter, velocity v_d results from Eq. 6, whereas

$$\boldsymbol{\vartheta}(\boldsymbol{p}) = \begin{bmatrix} \vartheta_x(\boldsymbol{p}) \\ \vartheta_y(\boldsymbol{p}) \end{bmatrix} \triangleq \frac{\boldsymbol{w}(\boldsymbol{p})}{\|\nabla F(\boldsymbol{p})\|} \tag{17}$$

is a normalized vector of the negative gradient of function $F(\boldsymbol{p})$, well defined for all $\boldsymbol{p} \in \mathcal{D}$ (see assumptions A1-A2).

In order to define the angular component h_θ of the vector field (11), let us introduce the auxiliary orientation angle

$$\theta_a(\boldsymbol{p}) \triangleq \mathrm{Atan2c}\left(\zeta_d h_y(\boldsymbol{p}), \zeta_d h_x(\boldsymbol{p})\right) \in \mathbb{R}, \tag{18}$$

where the operator[2] $\mathrm{Atan2c}(\cdot,\cdot) : \mathbb{R}\times\mathbb{R} \to \mathbb{R}$ is a continuous counterpart of the four-quadrant function $\mathrm{Atan2}(\cdot,\cdot) : \mathbb{R}\times\mathbb{R} \to [-\pi, \pi)$, and the auxiliary orientation error

$$e_a(\boldsymbol{q}) \triangleq \theta_a(\boldsymbol{p}) - \theta, \qquad e_a(\boldsymbol{q}) \in \mathbb{R}. \tag{19}$$

Following [9] and [21], we propose to define

$$h_\theta(\boldsymbol{q}) \triangleq k_a e_a(\boldsymbol{q}) + \dot{\theta}_{an}(\boldsymbol{q}) \tag{20}$$

[2] Implementation of operator $\mathrm{Atan2c}(\cdot,\cdot)$, when its arguments are defined in the discrete-time domain, can be found in Appendix D; see also [9]. In the continuous-time domain, an action of operator $\mathrm{Atan2c}(\cdot,\cdot)$ in Eq. 18 corresponds to the integral $\theta_a(t) = \theta_a(0) + \int_0^t \dot{\theta}_a(\xi) d\xi$, where the form of $\dot{\theta}_a$ has been provided in Appendix C.

where $k_a > 0$ is a second design parameter, while

$$\dot{\theta}_{an}(\boldsymbol{q}) \triangleq \frac{\dot{h}_{yn}(\boldsymbol{q})h_x(\boldsymbol{p}) - h_y(\boldsymbol{p})\dot{h}_{xn}(\boldsymbol{q})}{h_x^2(\boldsymbol{p}) + h_y^2(\boldsymbol{p})} \tag{21}$$

is the *nominal* feedforward term. The *nominal* time derivatives $\dot{h}_{xn}$ and $\dot{h}_{yn}$ used in Eq. 21 result from the following equation

$$\begin{aligned}\dot{\overline{\boldsymbol{h}}}_n(\boldsymbol{q}) &= \begin{bmatrix} \dot{h}_{xn}(\boldsymbol{q}) \\ \dot{h}_{yn}(\boldsymbol{q}) \end{bmatrix} \\ &\overset{(16)}{=} v_d \boldsymbol{R}\dot{\boldsymbol{\vartheta}}_n(\boldsymbol{q}) + k_p[\dot{F}_n(\boldsymbol{q})\boldsymbol{\vartheta}(\boldsymbol{p}) + F(\boldsymbol{p})\dot{\boldsymbol{\vartheta}}_n(\boldsymbol{q})] \\ &= \begin{bmatrix} v_d\dot{\vartheta}_{yn}(\boldsymbol{q}) + k_p[\dot{F}_n(\boldsymbol{q})\vartheta_x(\boldsymbol{p}) + F(\boldsymbol{p})\dot{\vartheta}_{xn}(\boldsymbol{q})] \\ -v_d\dot{\vartheta}_{xn}(\boldsymbol{q}) + k_p[\dot{F}_n(\boldsymbol{q})\vartheta_y(\boldsymbol{p}) + F(\boldsymbol{p})\dot{\vartheta}_{yn}(\boldsymbol{q})] \end{bmatrix},\end{aligned} \tag{22}$$

where (omitting the arguments for the sake of compactness)

$$\begin{aligned}\dot{F}_n &\triangleq \frac{\partial F}{\partial \boldsymbol{p}} \begin{bmatrix} \dot{x} \\ \dot{y} \end{bmatrix}\Bigg|_{\boldsymbol{u}=\boldsymbol{u}_n} \\ &\overset{(1)}{=} (F_x \mathrm{c}\theta + F_y \mathrm{s}\theta) u_{2n} \\ &\overset{(13)}{=} (F_x \mathrm{c}\theta + F_y \mathrm{s}\theta) u_2^{\mathrm{VFO}} \\ &\overset{(12)}{=} (F_x \mathrm{c}\theta + F_y \mathrm{s}\theta)(h_x \mathrm{c}\theta + h_y \mathrm{s}\theta)\end{aligned} \tag{23}$$

and

$$\begin{aligned}\dot{\boldsymbol{\vartheta}}_n &= \begin{bmatrix} \dot{\vartheta}_{xn} \\ \dot{\vartheta}_{yn} \end{bmatrix} \triangleq \frac{\partial \boldsymbol{\vartheta}}{\partial \boldsymbol{p}} \begin{bmatrix} \dot{x} \\ \dot{y} \end{bmatrix}\Bigg|_{\boldsymbol{u}=\boldsymbol{u}_n} \\ &\overset{(17,1)}{=} u_{2n} \begin{bmatrix} F_y(\eta_1 \mathrm{c}\theta + \eta_2 \mathrm{s}\theta)/\| \nabla F\|^3 \\ F_x(\eta_3 \mathrm{c}\theta + \eta_4 \mathrm{s}\theta)/\| \nabla F\|^3 \end{bmatrix} \\ &\overset{(13)}{=} \frac{u_2^{\mathrm{VFO}}}{\| \nabla F\|^3} \begin{bmatrix} F_y(\eta_1 \mathrm{c}\theta + \eta_2 \mathrm{s}\theta) \\ F_x(\eta_3 \mathrm{c}\theta + \eta_4 \mathrm{s}\theta) \end{bmatrix} \\ &\overset{(12)}{=} \frac{h_x \mathrm{c}\theta + h_y \mathrm{s}\theta}{\| \nabla F\|^3} \begin{bmatrix} F_y(\eta_1 \mathrm{c}\theta + \eta_2 \mathrm{s}\theta) \\ F_x(\eta_3 \mathrm{c}\theta + \eta_4 \mathrm{s}\theta) \end{bmatrix}\end{aligned} \tag{24}$$

with $\boldsymbol{p} = [x\ y]^\top$ (see Eq. 2), and $\eta_1 = F_x F_{xy} - F_y F_{xx}$, $\eta_2 = F_x F_{yy} - F_y F_{xy}$, $\eta_3 = F_y F_{xx} - F_x F_{xy}$, $\eta_4 = F_y F_{xy} - F_x F_{yy}$. The time derivatives indexed by subscript n and defined by Eqs. 23 and 24 indicate that they are computed upon velocities $\dot{x}$ and $\dot{y}$ obtained from kinematics (1) driven by the *nominal* control input $\boldsymbol{u} = \boldsymbol{u}_n = \boldsymbol{u}^{\mathrm{VFO}}$ (see Eq. 13), that is, without taking into account any control input constraints. This notational distinction is crucial for proper analysis of the closed-loop dynamics after considering control input constraints using a scaling procedure proposed in Section 3.3.

Remark 2 According to definition (16) and due to assumption A3 one can easily verify that

$$\det\left(v_d \boldsymbol{R} + k_p F(\boldsymbol{p}) \boldsymbol{I}_{2\times 2}\right) = k_p^2 F^2(\boldsymbol{p}) + v_d^2 \geq v_d^2 > 0.$$

Thus, the vector field (16), and consequently the auxiliary angle (18) with nominal time derivative (21), are well determined if only $\| \nabla F(\boldsymbol{p})\| \neq 0$. The latter condition is satisfied for all $\boldsymbol{p} \in \mathcal{D}$ under assumption A2.

Remark 3 Parametric synthesis of the VFO controller involves selection of only two positive values for parameters k_p and k_a. Previous experience with the VFO controllers devised for the trajectory tracking and set-point control tasks, see [9, 22], may suggest selection of k_p and k_a according to a simple design rule: $k_a > k_p$, and in particular $k_a = 2k_p$. Selection of k_p shall result from a compromise between a desirable *rigidity* of the controller on one hand, and dominant practical limitations on the other hand, caused usually by the presence of a measurement noise in a feedback loop or by the time delays affecting a control loop. Based on the previous experience, one may suggest to take (at least initially) $k_p \in [1, 5]$.

3.3 Control Input Scaling

The nominal control law (13) does not take into account control input limitations resulting from the prescribed condition (4). Satisfaction of constraint (4) can be guaranteed by application of the so-called Velocity Scaling Block (VSB) utilized, e.g., in [9, 22]. The working principles of the VSB can be explained as follows. Assume that the *nominal* control input $\boldsymbol{u}_n = [u_{1n}\ u_{2n}]^\top$ has been computed for kinematics (1) according to Eq. 13. An action of the VSB is determined as a post-processing of the nominal control input by taking

$$\boldsymbol{u}_s(t) = \begin{bmatrix} u_{1s}(t) \\ u_{2s}(t) \end{bmatrix} \triangleq \varsigma(t)\boldsymbol{u}_n(t) \overset{(13)}{=} \varsigma(t)\boldsymbol{u}^{\mathrm{VFO}}(t), \tag{25}$$

where $\boldsymbol{u}_s$ is a scaled control input, $\varsigma(t)$ is a scaling function defined as

$$\varsigma(t) \triangleq \left[\max\left\{1; \frac{|\omega_{rn}(t)|}{\omega_m}; \frac{|\omega_{ln}(t)|}{\omega_m}\right\}\right]^{-1} \in (0, 1], \tag{26}$$

while velocities $\boldsymbol{\Omega}_n = [\omega_{rn}\ \omega_{ln}]^\top$ are obtained by applying (3), that is,

$$\boldsymbol{\Omega}_n = \boldsymbol{J}^{-1}\boldsymbol{u}_n \overset{(13)}{=} \boldsymbol{J}^{-1}\boldsymbol{u}^{\mathrm{VFO}}. \tag{27}$$

It is worth to emphasize that scaled control input $\boldsymbol{u}_s$ applied into kinematics (1) ensures, by construction, satisfaction of constraint (4), simultaneously preserving an instantaneous nominal motion curvature, that is, $u_{1s}/u_{2s} = u_{1n}/u_{2n}$, see [9]. The latter property assures a well predictable transient motion of a robot despite reaching the control input limitations. Location of the Velocity Scaling Block in a resultant control system has been clarified by the block scheme in Fig. 2.

According to definition (26), it is evident that for $\omega_m > 0$ and for any bounded nominal control $\boldsymbol{u}_n$ there exists a lower bound

$$\underline{\varsigma} \triangleq \inf_{t\geq 0}[\varsigma(t)] > 0. \tag{28}$$

The lower bound $\underline{\varsigma}$ defined above will be utilized in the stability analysis in Section 3.4.

3.4 The Main Result

The main result of the paper can be formulated by the following theorem.

Theorem 1 *The VFO control law (25), with the nominal term (12) determined for the convergence vector field defined by Eqs. 16 and 20, applied into kinematics (1) by taking*

$$\boldsymbol{u}(t) := \boldsymbol{u}_s(t) \overset{(25)}{=} \varsigma(t)\boldsymbol{u}^{VFO}(t) \overset{(12)}{=} \varsigma(t)\begin{bmatrix} h_\theta(t) \\ \boldsymbol{h}(t)^\top \boldsymbol{g}_2(\theta(t)) \end{bmatrix} \tag{29}$$

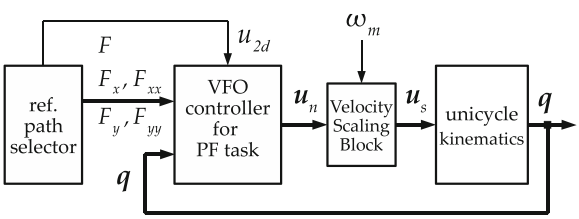

Fig. 2 A block scheme of the proposed VFO control system explaining location of the Velocity Scaling Block

solves the Positionally Constrained PF Problem ensuring that $\forall t \geq 0\ e_F(\boldsymbol{p}(t)) \in \mathcal{D}_F^*$ *for any prescribed subset*

$$\mathcal{D}_F^* \triangleq (-r_F, r_F) \quad with \quad 0 < r_F \leq \min\{|\underline{F}|, \overline{F}\}, \tag{30}$$

if the initial errors satisfy

$$\boldsymbol{e}(\boldsymbol{q}(0)) \in [-\pi, \pi)\times(-r_f, r_f) \ \wedge\ |e_{a0}| \triangleq |e_a(\boldsymbol{q}(0))| < r_a$$

for the bounds r_f *and* r_a *taken as a one of two alternative pairs of values*

$$\begin{aligned} &(p1) \quad r_f = r_F, && r_a = r_1^* \\ &(p2) \quad r_f = r_F/\sqrt{1+\mu e_{a0}^2}, && r_a = r_2^* \end{aligned}$$

with r_1^* *and* r_2^* *being positive roots of respective equations*

$$\begin{aligned} &P_1(r_1^*) = 0, \quad P_1(r) = \frac{r}{\cos^2 r} - \phi \\ &P_2(r_2^*) = 0, \quad P_2(r) = \mu^3 r^8 + 3\mu^2 r^6 + 3\mu r^4 + r^2 - \phi^2 \end{aligned}$$

where $\mu = (\underline{m}k_p/k_a) > 0$, $\phi = (r_F k_p \underline{m}\nu/v_d\overline{m}) > 0$, *while* $\nu \in (0, 1)$ *is a prescribed constant.*

Remark 4 The two pairs, *(p1)* and *(p2)*, of bounds r_f and r_a determine different conservativeness degrees of the proposed solution. In particular, the pair *(p1)* admits the initial positional error from the whole prescribed set $\mathcal{D}_F^*$, but it confines the admissible initial error $|e_{a0}|$ to the range not exceeding the value of r_1^* which is always less than $\pi/2$ rad (since ϕ is finite upon assumptions A1-A3). On the other hand, the upper bound r_2^* in the pair *(p2)* is, in general, not limited by the value of $\pi/2$ rad (generally admitting larger initial error $|e_{a0}|$), but at the expense of the more conservative bound r_f imposed on the positional error (with the term e_{a0}^2 in the denominator). Two above pairs of the upper bounds have been intentionally provided to allow for more flexible usage of the proposed solution in various practical circumstances. Namely, if the initial errors do not meet constraints for the upper bounds from pair *(p1)*, one can alternatively check satisfaction of the constraints for the pair *(p2)*. For example, prescribing $r_F = 2.8$, $\phi = 9.4$, and $\mu = 0.5$ (cf. conditions of example SimII in Section 4), and postulating $|e_{a0}| = 1.5$ rad, the pair

(p1) returns $r_f = 2.8, r_a \approx 1.21$ rad while *(p2)* gives $r_f \approx 1.92$ and $r_a \approx 1.93$ rad. Thus in this particular case, the auxiliary initial error e_{a0} does not satisfy constraints imposed by *(p1)*, but the Positionally Constrained PF Problem can still be resolved upon *(p2)* if only the initial positional error $|e_F(\boldsymbol{p}(0))| < 1.92$.

Proof of Theorem 1 Let us first consider closed-loop dynamics of the auxiliary orientation error. Upon definitions (19), (20), (29), and according to the first equation of Eq. 1 one can write:

$$\begin{aligned}\dot{e}_a &\overset{(19)}{=} \dot{\theta}_a - \dot{\theta} \overset{(1)}{=} \dot{\theta}_a - u_1 \overset{(29)}{=} \dot{\theta}_a - \varsigma h_\theta \\ &\overset{(20)}{=} \dot{\theta}_a - \varsigma k_a e_a - \varsigma \dot{\theta}_{an} = -\varsigma k_a e_a \end{aligned} \tag{31}$$

where we have used the fact $\dot{\theta}_a = \varsigma \dot{\theta}_{an}$ (see Appendix C). Defining a positive definite function $V_1(e_a) \triangleq \frac{1}{2} e_a^2$, one can assess its time derivative as

$$\dot{V}_1 = e_a \dot{e}_a \overset{(31)}{=} -\varsigma k_a e_a^2 \leq -\underline{\varsigma} k_a e_a^2 = -2\underline{\varsigma} k_a V_1, \tag{32}$$

where the lower bound $\underline{\varsigma}$ comes from Eq. 28. According to Eq. 32, and by the Comparison Lemma [11], one concludes

$$|e_a(\boldsymbol{q}(t))| \leq |e_{a0}| \exp(-\underline{\varsigma} k_a t), \qquad e_{a0} = e_a(\boldsymbol{q}(0)), \tag{33}$$

for all $t \geq 0$, and upon (31)

$$\sup_{t \geq 0} |e_a(\boldsymbol{q}(t))| = |e_{a0}|. \tag{34}$$

Next, we are going to analyze closed-loop dynamics of the positional error component $e_F(\boldsymbol{p}) \equiv F(\boldsymbol{p})$, see Eq. 9. The set $\mathcal{D}_F^*$ defined by Eq. 30 imposes a limit on an admissible domain of the positional error, that is,

$$e_F \in \mathcal{D}_F^* \quad \Rightarrow \quad |e_F| < r_F. \tag{35}$$

By expressing the control component $u_2(t)$ of Eq. 29 in its equivalent form $u_2(t) = \varsigma(t) \zeta_d \| \bar{\boldsymbol{h}}(t) \| \mathrm{c} e_a(t)$ (see Appendix A), and using definition (16), one may show (see Appendix B) that the closed-loop dynamics of error $e_F(\boldsymbol{p})$ satisfies the following equation (omitting the arguments for clarity)

$$\dot{e}_F = -\varsigma\, k_p \mathrm{c}^2 e_a \| \nabla F \| e_F + \varsigma\, v_d \mathrm{s} e_a \mathrm{c} e_a \| \nabla F \|,$$

where $\varsigma = \varsigma(t)$ is a scaling function defined by Eq. 26. Combination of the above equation with Eq. 31 gives cascade dynamics

$$\dot{e}_F = -\varsigma\, k_p \mathrm{c}^2 e_a \| \nabla F \| e_F + \varsigma\, v_d \mathrm{s} e_a \mathrm{c} e_a \| \nabla F \|, \tag{36}$$

$$\dot{e}_a = -\varsigma\, k_a e_a, \tag{37}$$

for which the pair $(e_F, e_a) = (0, 0)$ is the only equilibrium, and point $e_a = 0$ of dynamics (37) is globally exponentially stable according to Eq. 33. Now, one can treat the term e_a in Eq. 36 as a *perturbing input*, where $\dot{e}_F = -\varsigma\, k_p \| \nabla F \| e_F$ for $e_a = 0$.

We will proceed further considerations independently for the two alternative pairs *(p1)* and *(p2)* of bounds r_f and r_a introduced in Theorem 1. They will be subsequently presented in the next two paragraphs, followed next by a continued common analysis. In the sequel, we will utilize the concept of input-to-state stability [32] which has been shortly recalled in Appendix E.

Analysis Concerning the Pair (p1) Let us define a positive definite function $V_2 : \mathcal{D}_F^* \to \mathbb{R}_{\geq 0}$ of the form

$$V_2(e_F) \triangleq \frac{1}{2} e_F^2, \tag{38}$$

which satisfies $\alpha_1(|e_F|) \leq V(e_F) \leq \alpha_2(|e_F|)$ for the $\mathcal{K}$-class functions

$$\alpha_1(|e_F|) = \alpha_2(|e_F|) = |e_F|^2 / 2. \tag{39}$$

One can estimate a time derivative of $V_2(e_F)$ as follows:

$$\begin{aligned}\dot{V}_2 = e_F \dot{e}_F &\overset{(36)}{=} -\varsigma k_p \mathrm{c}^2 e_a \| \nabla F \| e_F^2 + \varsigma v_d \mathrm{s} e_a \mathrm{c} e_a \| \nabla F \| e_F \\ &\leq -\varsigma k_p \delta_a \underline{m}\, e_F^2 + \varsigma v_d \overline{m}\, |e_a|\, |e_F| \\ &\quad + \varsigma k_p \delta_a \underline{m}\, \nu e_F^2 - \varsigma k_p \delta_a \underline{m}\, \nu e_F^2 \\ &\leq -\underline{\varsigma} k_p \delta_a \underline{m}\, (1-\nu) e_F^2 + \varsigma \underbrace{(v_d \overline{m}\, |e_a|\, |e_F| - k_p \delta_a \underline{m}\, \nu e_F^2)}_{W(e_F, e_a)} \end{aligned} \tag{40}$$

where $\nu \in (0, 1)$ is a majorization constant, the bounds $\underline{m}$, $\overline{m}$, and constant $\underline{\varsigma}$ result from assumption A2 and Eq. 28, respectively, while

$$\delta_a \triangleq \mathrm{c}^2 (\sup_{t \geq 0} |e_a(\boldsymbol{q}(t))|) = \mathrm{c}^2 |e_{a0}| > 0 \quad \text{for} \quad |e_{a0}| < \frac{\pi}{2} \tag{41}$$

has been determined upon (34). According to Eq. 40, one observes that $\dot{V}_2 \leq 0$ if the term $W(e_F, e_a)$ is non-positive. In particular, one may conclude that

$$\dot{V}_2 \leq -\underline{\varsigma} k_p \delta_a \underline{m}\, (1 - \nu) e_F^2 \quad \text{for} \quad |e_F| \geq \chi(|e_a|) \tag{42}$$

where

$$\chi(|e_a|) = \frac{v_d \overline{m}}{k_p \delta_a \underline{m} \nu} |e_a|, \tag{43}$$

is a function of class $\mathcal{K}$ upper bounded by (see Eq. 34)

$$\sup_{t\geq 0} \chi(|e_a(\boldsymbol{q}(t))|) = \chi(|e_{a0}|) = \frac{v_d \overline{m}}{k_p \delta_a \underline{m} \nu} |e_{a0}|. \tag{44}$$

As a consequence of Eq. 42, one concludes that dynamics (36) is locally ISS (*Input-to-State Stable*, see Appendix E) with respect to *input* e_a satisfying

$$|e_F(\boldsymbol{p}(t))| \leq \max\left\{\beta(|e_F(\boldsymbol{p}(0))|, t); \gamma\left(\sup_{t\geq 0}|e_a(\boldsymbol{q}(t))|\right)\right\} \overset{(34)}{=} \max\{\beta(|e_F(\boldsymbol{p}(0))|, t); \gamma(|e_{a0}|)\} \tag{45}$$

for all $t \geq 0$, where $\beta(\cdot,\cdot)$ is a function of class $\mathcal{KL}$, while

$$\gamma(|e_a|) = \alpha_1^{-1}[\alpha_2(\chi(|e_a|))] \overset{(39)}{=} \chi(|e_a|) \overset{(43)}{=} \frac{v_d \overline{m}\,|e_a|}{k_p \delta_a \underline{m} \nu}. \tag{46}$$

In the light of constraints determined by Eqs. 35 and 41, the ISS result (45) is valid locally for the initial positional error (cf. Appendix E)

$$|e_F(\boldsymbol{p}(0))| < r_f, \quad r_f = \alpha_2^{-1}[\alpha_1(r_F)] \overset{(39)}{=} r_F \tag{47}$$

and the supremum (34) of the perturbing input satisfying

$$|e_{a0}| < \chi^{-1}\left(\min\left\{r_f, \chi(\pi/2)\right\}\right) \overset{(47)}{=} \chi^{-1}\left(\min\left\{r_F, \chi(\pi/2)\right\}\right). \tag{48}$$

According to the form of Eq. 43 and recalling definition from Eq. 41, the inequality (48) can be rewritten as

$$\frac{|e_{a0}|}{c^2|e_{a0}|} < \frac{r_F k_p \underline{m} \nu}{v_d \overline{m}} \quad \wedge \quad |e_{a0}| < \frac{\pi}{2}, \tag{49}$$

which gives the resultant condition

$$|e_{a0}| < r_a = r_1^* \tag{50}$$

where $r_1^* < \pi/2$ is a positive root of equation

$$\frac{r}{\cos^2 r} - \frac{r_F k_p \underline{m} \nu}{v_d \overline{m}} = 0. \tag{51}$$

Since $r/\cos^2 r$ is a monotonic function, and $\frac{r_F k_p \underline{m} \nu}{v_d \overline{m}} > 0$ is a finite constant, a positive root of Eq. 51 will be always less than $\pi/2$ satisfying the second inequality postulated in Eq. 49.

According to Eq. 45, one concludes uniform boundedness of positional error $e_F(\boldsymbol{p}(t))$ which belongs to the set $\mathcal{D}_F^*$ for all $t \geq 0$ if initial errors $|e_F(\boldsymbol{p}(0))|$ and $|e_a(\boldsymbol{q}(0))|$ satisfy conditions (47) and (50), respectively. Upon definition (9), one concludes uniform boundedness of $\|\boldsymbol{e}(\boldsymbol{q}(t))\|$. Furthermore, the ISS property reflected by Eq. 45 corresponds to satisfaction of the *asymptotic gain* relation (see e.g. [10, 31]):

$$\limsup_{t\to\infty} |e_F(\boldsymbol{p}(t))| \leq \gamma\left(\limsup_{t\to\infty} |e_a(\boldsymbol{q}(t))|\right) \overset{(46)}{=} \frac{v_d \overline{m}}{k_p \delta_a \underline{m} \nu} \limsup_{t\to\infty} |e_a(\boldsymbol{q}(t))| \overset{(33)}{=} 0. \tag{52}$$

Hence, one concludes that the equilibrium $(e_F, e_a) = (0,0)$ of cascade dynamics (36)–(37) is locally asymptotically stable for any initial condition $(e_F(\boldsymbol{p}(0)), e_a(\boldsymbol{q}(0)))$ from the set $(-r_F, r_F) \times (-r_a, r_a)$ with r_a determined by Eq. 50.

Analysis Concerning the Pair (p2) Let us define an auxiliary time-dependent function

$$f_a(t) : [0,\infty) \to \mathbb{R} \tag{53}$$

which is a solution of the differential equation

$$\dot{f}_a(t) = -\varsigma k_a f_a(t) \tag{54}$$

for the initial condition $f_a(0) \triangleq e_{a0}$. Thus, by comparing (54) with (31) one observes

$$\forall\, t \geq 0 \;\; f_a(t) = e_a(\boldsymbol{q}(t)). \tag{55}$$

Define a function $V_2 : \mathcal{D}_F^* \times [0,\infty) \to \mathbb{R}_{\geq 0}$ of the form

$$V_2(e_F, t) \triangleq \frac{1}{2} e_F^2 (1 + \mu f_a^2(t)), \quad \mu = \frac{\underline{m} k_p}{k_a} > 0. \tag{56}$$

For all $t \geq 0$, the function (56) is positive definite, $V_2(0,t) \equiv 0$, and

$$\alpha_1(|e_F|) \leq V_2(e_F, t) \leq \alpha_2(|e_F|) \tag{57}$$

for the $\mathcal{K}$-class functions

$$\alpha_1(|e_F|) = \frac{|e_F|^2}{2}, \quad \alpha_2(|e_F|) = \frac{|e_F|^2 (1 + \mu e_{a0}^2)}{2}. \tag{58}$$

A time derivative of $V_2(e_F, t)$ can be estimated as follows:

$$\begin{aligned}\dot{V}_2 &= e_F\dot{e}_F(1+\mu f_a^2)+\mu e_F^2 f_a\dot{f}_a\\ &\overset{(36)}{=}(1+\mu f_a^2)\left[-\varsigma k_p \mathrm{c}^2 e_a\|\nabla F\|e_F^2+\varsigma v_d \mathrm{s}e_a \mathrm{c}e_a\|\nabla F\|e_F\right]\\ &\quad+\mu e_F^2 f_a\dot{f}_a\\ &\overset{(54)}{=}(1+\mu f_a^2)\left[-\varsigma k_p \mathrm{c}^2 e_a\|\nabla F\|e_F^2+\varsigma v_d \mathrm{s}e_a \mathrm{c}e_a\|\nabla F\|e_F\right]\\ &\quad-\mu\varsigma k_a e_F^2 f_a^2\\ &\leq -\varsigma k_p \mathrm{c}^2 e_a \underline{m} e_F^2+(1+\mu e_{a0}^2)\varsigma v_d\,|e_a|\,\overline{m}\,|e_F|-\mu\varsigma k_a e_F^2 e_a^2\end{aligned}$$

where we have utilized equality (55), while the bounds $\underline{m}$ and $\overline{m}$ result from assumption A2. Recalling the form of coefficient μ (see Eq. 56), and utilizing the fact $e_a^2 \geq \mathrm{s}^2 e_a = 1-\mathrm{c}^2 e_a$, one may proceed the above estimation by writing

$$\begin{aligned}\dot{V}_2 &\leq -\varsigma k_p \underline{m}\,\mathrm{c}^2 e_a e_F^2+(1+\mu e_{a0}^2)\varsigma v_d\,\overline{m}\,|e_a|\,|e_F|\\ &\quad-\varsigma k_p \underline{m}\,e_F^2(1-\mathrm{c}^2 e_a)+\varsigma k_p \underline{m}\,\nu e_F^2-\varsigma k_p \underline{m}\,\nu e_F^2\\ &\leq -\underline{\varsigma} k_p \underline{m}\,(1-\nu)e_F^2\\ &\quad+\varsigma\underbrace{[(1+\mu e_{a0}^2)v_d\,\overline{m}\,|e_a|\,|e_F|-k_p \underline{m}\,\nu e_F^2]}_{W(e_F,e_a)},\end{aligned}\tag{59}$$

where $\nu \in (0,1)$ is a prescribed majorization constant. According to Eq. 59, one observes that $\dot{V}_2 \leq 0$ if the term $W(e_F, e_a)$ is non-positive. In particular, one may conclude that

$$\dot{V}_2 \leq -\underline{\varsigma} k_p \underline{m}\,(1-\nu)e_F^2 \quad \text{for} \quad |e_F| \geq \chi(|e_a|),\tag{60}$$

where

$$\chi(|e_a|)=\frac{v_d\overline{m}(1+\mu e_{a0}^2)}{k_p \underline{m}\nu}\,|e_a|\,,\tag{61}$$

is a function of class $\mathcal{K}$ upper bounded by (see Eq. 34)

$$\sup_{t\geq 0}\chi(|e_a(\boldsymbol{q}(t))|)=\chi(|e_{a0}|)=\frac{v_d\overline{m}}{k_p\underline{m}\nu}|e_{a0}|(1+\mu|e_{a0}|^2).\tag{62}$$

According to Eq. 60, one may conclude that dynamics (36) is locally ISS (*Input-to-State Stable*, see Appendix E) with respect to *input* e_a satisfying

$$\begin{aligned}|e_F(\boldsymbol{p}(t))| &\leq \max\left\{\beta(|e_F(\boldsymbol{p}(0))|,t);\gamma\left(\sup_{t\geq 0}|e_a(\boldsymbol{q}(t))|\right)\right\}\\ &\overset{(34)}{=}\max\{\beta(|e_F(\boldsymbol{p}(0))|,t);\gamma(|e_{a0}|)\}\end{aligned}\tag{63}$$

for all $t \geq 0$, where $\beta(\cdot,\cdot)$ is a function of class $\mathcal{KL}$, while

$$\gamma(|e_a|)=\alpha_1^{-1}[\alpha_2(\chi(|e_a|))]\overset{(58)}{=}\frac{v_d\overline{m}\,|e_a|}{k_p\underline{m}\nu}(1+\mu e_{a0}^2)^{3/2}.\tag{64}$$

Due to constraint (35), the ISS result (63) is valid locally for the initial positional error (cf. Appendix E)

$$|e_F(\boldsymbol{p}(0))|<r_f,\quad r_f=\alpha_2^{-1}[\alpha_1(r_F)]\overset{(58)}{=}\frac{r_F}{\sqrt{1+\mu e_{a0}^2}}\tag{65}$$

and the supremum (34) of the perturbing input satisfying

$$|e_{a0}|<\chi^{-1}(r_f)\overset{(61)}{=}\frac{k_p\underline{m}\nu}{v_d\overline{m}}\cdot\frac{r_F}{(1+\mu\,|e_{a0}|^2)^{3/2}},$$

where the form of r_f in the above inequality has been taken from Eq. 65. Because both the left- and right-hand sides of the above inequality depend on $|e_{a0}|$, one has to resolve it with respect to $|e_{a0}|$. As a consequence, the resultant condition on the initial auxiliary error takes the form

$$|e_{a0}|<r_a=r_2^*\tag{66}$$

where r_2^* is a positive real root of equation

$$\mu^3 r^8+3\mu^2 r^6+3\mu r^4+r^2-\left(\frac{r_F k_p\underline{m}\nu}{v_d\overline{m}}\right)^2=0.\tag{67}$$

Since $\mu > 0$ (cf. Eq. 56), there will be only a single positive root of Eq. 67 according to the Descartes' Sign Rule.

As a consequence of Eq. 63, one concludes uniform boundedness of positional error $e_F(\boldsymbol{p}(t))$, which is confined to the set $\mathcal{D}_F^*$ for all $t \geq 0$ if initial errors $|e_F(\boldsymbol{p}(0))|$ and $|e_a(\boldsymbol{q}(0))|$ satisfy conditions (65) and (66), respectively. Due to definition (9), one concludes uniform boundedness of $\|\boldsymbol{e}(\boldsymbol{q}(t))\|$. Furthermore, the ISS property reflected by inequality (63) implies satisfaction of the following *asymptotic gain* relation:

$$\begin{aligned}\limsup_{t\to\infty}|e_F(\boldsymbol{p}(t))| &\leq \gamma\left(\limsup_{t\to\infty}|e_a(\boldsymbol{q}(t))|\right)\\ &\overset{(64)}{=}\frac{v_d\overline{m}(1+\mu e_{a0}^2)^{3/2}}{k_p\underline{m}\nu}\limsup_{t\to\infty}|e_a(\boldsymbol{q}(t))|\overset{(33)}{=}0.\end{aligned}\tag{68}$$

Hence, one concludes that the equilibrium $(e_F, e_a) = (0,0)$ of cascade dynamics (36)–(37)

is locally asymptotically stable for any initial condition $(e_F(\boldsymbol{p}(0)), e_a(\boldsymbol{q}(0)))$ from the set $(-r_f, r_f) \times (-r_a, r_a)$ with r_f and r_a determined by Eqs. 65 and 66, respectively.

Continued Common Analysis Now, upon (52) and (68), together with definitions (9) and (5), one may conclude that

$$e_F(\boldsymbol{p}(t)) \overset{t\to\infty}{\longrightarrow} 0 \quad \Rightarrow \quad \mathrm{D}(\boldsymbol{p}(t), S_d) \overset{t\to\infty}{\longrightarrow} 0, \tag{69}$$

where $\mathrm{D}(\boldsymbol{p}, S_d) \triangleq \inf_{\boldsymbol{p}_d \in S_d} \| \boldsymbol{p}_d - \boldsymbol{p} \|$ is a distance from point $\boldsymbol{p}$ to set S_d. In view of Eq. 69, and according to definitions (18) and (16), one obtains

$$\begin{aligned} \theta_a(\boldsymbol{p}) \overset{\mathrm{D}(\boldsymbol{p},S_d)\to 0}{\longrightarrow} \theta_a(\boldsymbol{p}_d) &= \mathrm{Atan2c}\left(\zeta_d F_x(\boldsymbol{p}_d), -\zeta_d F_y(\boldsymbol{p}_d)\right) \\ &\overset{(7)}{=} \theta_d(\boldsymbol{p}_d) \mod 2\pi, \end{aligned} \tag{70}$$

what, in the light of Eq. 33 together with definition (9), implies $e_\theta(t) \overset{t\to\infty}{\longrightarrow} 0$.

Finally, by recalling definitions (25), (16), (20), (21), and (6), one may observe that both $|e_F(\boldsymbol{p})| < \infty$ and assumption A3 imply $\| \overline{\boldsymbol{h}}(\boldsymbol{p}) \| < \infty$, and (as a consequence) boundedness of $u_2(\boldsymbol{q})$. Next, $|u_2(\boldsymbol{q})| < \infty$ together with $|e_a(\boldsymbol{q})| < \infty$ and $\| \overline{\boldsymbol{h}}(\boldsymbol{p}) \| < \infty$ imply (under assumptions A1 and A2) boundedness of $h_\theta(\boldsymbol{q})$, and (as a consequence) boundedness of $u_1(\boldsymbol{q})$. Moreover, for $(e_F, e_a) \to (0, 0)$ the following relations hold true: $u_1 \to \dot{\theta}_d$ and $u_2 \to \zeta_d \| \overline{\boldsymbol{h}}(\boldsymbol{p}_d) \| = \zeta_d v_d = u_{2d}$.

□

Remark 5 Worth to stress that values of bound r_a are expressed in radians, however a value of bound r_f is dimensionless because the error $|e_F(\boldsymbol{p})| = |F(\boldsymbol{p})|$ does not correspond, in general, to the Euclidean distance. The error $|e_F(\boldsymbol{p})|$ can be treated rather as a some (nonlinear) function of such a distance. On the other hand, by construction of function $F(\boldsymbol{p})$, see Eq. 5, it is possible to scale the values of this function and its slope by selecting an appropriate absolute value of coefficient σ. As a consequence, by intentional selection of $|\sigma|$ one may influence the resultant size of the prescribed set $\mathcal{D}_F^*$ and the corresponding geometrical neighborhood around a reference path expressible in metric units.

Remark 6 In the case when the initial error $|e_a(\boldsymbol{q}(0))|$ does not satisfy any of the upper bounds imposed by *(p1)* and *(p2)* in Theorem 1, one may initially apply (within some finite time interval $t \in [0, T]$) the *preparatory control* $\boldsymbol{u}_n(\boldsymbol{q}) := [h_\theta(\boldsymbol{q}) \; 0]^\top$ with $h_\theta(\boldsymbol{q})$ defined by Eq. 20, in order to preliminarily decrease the auxiliary orientation error to an acceptably small value $|e_a(\boldsymbol{q}(T))| < r_a$ with r_a taken either from *(p1)* or *(p2)*, while keeping simultaneously the robot position fixed at $\boldsymbol{p}(0)$. Next, one can switch to the VFO control law (25) for the initial error $|e_{a0}| := |e_a(\boldsymbol{q}(T))|$ satisfying conditions of Theorem 1.

4 Numerical Examples

Results of two numerical examples, SimI and SimII, have been presented to illustrate efficiency of the proposed control law for various motion scenarios. The following common values have been selected for the controller parameters, reference velocity, and kinematic parameters of the robot: $k_p = 1.0$, $k_a = 2.0$, $v_d = 0.08$ m/s, $r_w = 0.02$ m, $b = 0.145$ m. The Velocity Scaling Block has been implemented using $\omega_m = 7.5$ rad/s, which corresponds to the maximal robot-body velocities $|u_1|_{\max} = 2.07$ rad/s and $|u_2|_{\max} = 0.15$ m/s.

4.1 Example SimI

The first example concerns following the so-called super-elliptic path represented by a zero-level curve of function (see Fig. 3a)

$$F(\boldsymbol{p}) = \sigma \left[\frac{x^4}{0.8^4} + \frac{y^4}{0.5^4} - 1 \right], \quad \sigma = +1, \tag{71}$$

where the positive coefficient σ determines the desired (reference) motion along the path in the counterclockwise direction. Function (71) is bounded from below by value $\underline{F} = -1.0$, while it is unbounded from above. However for any finite position $\boldsymbol{p}$, values of function (71) are also upper bounded by some $\overline{F}$ as required by assumption A1. For example, if $\boldsymbol{p} \in \mathcal{D} = [-2, 2] \times [-2, 2]$ one can check that $\overline{F} \approx 294.06$. Furthermore, the norm of gradient $\| \nabla F(\boldsymbol{p}) \|$ takes the zero value at $\boldsymbol{p} = \boldsymbol{0}$ (the isolated singularity point), while it is unbounded from above. However for any finite $\boldsymbol{p}$, values of $\| \nabla F(\boldsymbol{p}) \|$ are upper bounded by some value $\overline{m}$ as required by assumption A2. Hence, the properties of $\| \nabla F(\boldsymbol{p}) \|$ for function (71) suggest to limit the admissible set of positions $\boldsymbol{p}$ to some bounded subset $\mathcal{D}$ excluding the point $\boldsymbol{p} = \boldsymbol{0}$, as

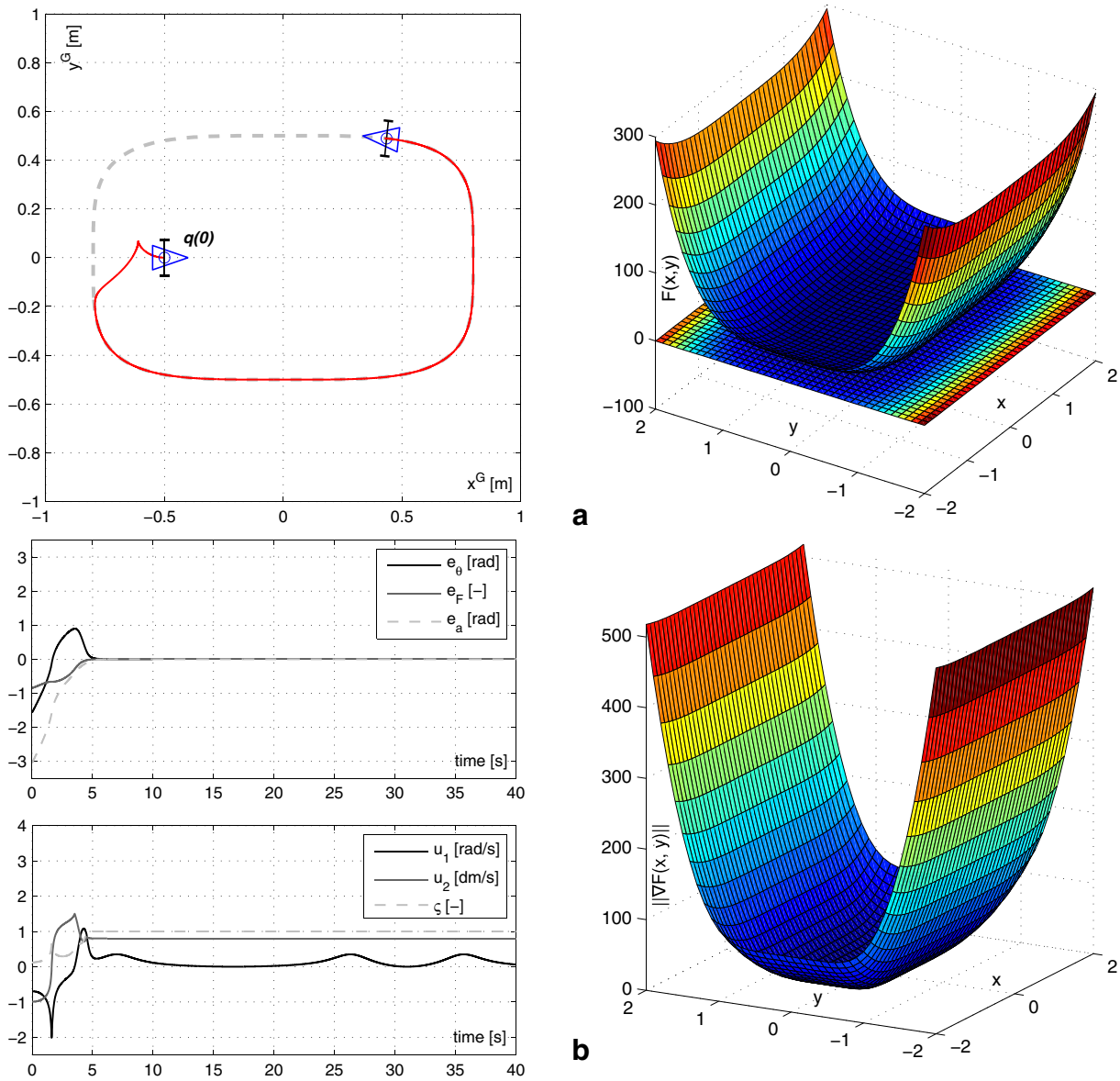

Fig. 3 SimI: control performance for the case of the superelliptic path followed in a forward motion strategy (*left column*), and the surfaces (*right column*) representing function $F(\boldsymbol{p})$, (**a**), and the norm of its gradient $\| \nabla F(\boldsymbol{p}) \|$, (**b**), for argument $\boldsymbol{p} \in [-2, 2] \times [-2, 2]$

required by assumption A2. For example, in the subset $\mathcal{D} = ([-2, 2] \setminus [-0.1, 0.1]) \times ([-2, 2] \setminus [-0.1, 0.1])$ one can verify (see Fig. 3b) that $\overline{m} \approx 517.93$ and $\underline{m} \approx 0.01$.

In the test SimI, the *forward* reference motion strategy has been assumed by taking $\zeta_d = +1$ (see Eq. 6). The initial robot configuration has been selected as $\boldsymbol{q}(0) = [0 \ \ -0.5 \ 0]^\top$. Results of the control process are presented by the plots in the left column in Fig. 3.

Analyzing the plots in Fig. 3 one can observe fast and non-oscillatory movement of the robot and fast transients of the path following errors asymptotically vanishing toward zero, despite relatively flat surface $F(\boldsymbol{p})$ in a neighborhood of the prescribed initial configuration. Transient evolution of particular errors can be additionally assessed upon the plot presented in Fig. 4, where the exponential rate of convergence can be clearly observed. Worth noting is the boundedness

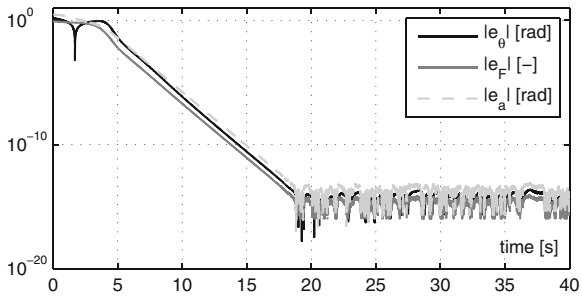

Fig. 4 SimI: absolute values of the path following errors and the auxiliary orientation error in a logarithmic scale

of the control inputs which satisfy control limitations resulting from the finite value of ω_m in the whole control time-horizon. Looking at the plot of $\varsigma(t)$, it is evident that the VSB (Velocity Scaling Block, see Section 3.3) modifies the control inputs only until about 5 s of a transient stage. Finally, it is worth to emphasize that the above control performance has been obtained despite relatively large values of the initial errors, that is, for $|e_a(\boldsymbol{q}(0))| \approx 3.05$ rad and $|e_F(\boldsymbol{p}(0))| \approx 0.85$. These numbers can be confronted with the estimates determined by pairs *(p1)* and *(p2)* in Theorem 1, which in this case have been computed as follows

$$(p1): r_f = r_F = 1.0, \quad r_a \approx 2.17 \cdot 10^{-4} \text{ rad}$$
$$(p2): r_f = \frac{r_F}{\sqrt{1+\mu(0.99 r_a)^2}} \approx 1.0, \quad r_a \approx 2.17 \cdot 10^{-4} \text{ rad}$$

by taking $r_F = |\underline{F}| = 1.0$ and $\nu = 0.9$. Satisfaction of the positionally constrained motion despite a large value of $|e_a(\boldsymbol{q}(0))|$ reveals conservativeness of conditions determined by *(p1)* and *(p2)*.

4.2 Example SimII

In the second example, we have considered the S-shaped path represented by a zero-level curve of the following function (see Fig. 5b)

$$F(\boldsymbol{p}) = \sigma\ [y - 0.8 \tanh(4x)], \quad \sigma = -1, \tag{72}$$

where the negative coefficient σ determines the desired (reference) motion along the path from the left-to-right direction. In this case, the function (72) is unbounded from above and from below, but for any finite position $\boldsymbol{p}$ the values of function (72) are lower and upper bounded (as required by assumption A1) by some finite values $\underline{F}$ and $\overline{F}$, respectively. For example, if $\boldsymbol{p} \in \mathcal{D} = [-2, 2] \times [-2, 2]$ one can check that $\overline{F} = -\underline{F} \approx 2.8$. On the other hand, the norm of gradient $\| \nabla F(\boldsymbol{p}) \|$ for function (72) is globally bounded satisfying assumption A2 for any $\boldsymbol{p} \in \mathbb{R}^2$ (no singular points) by finite values $\underline{m} = 1.0$ and $\overline{m} \approx 3.35$. Thus, the properties of function (72) allows limiting the admissible set of positions $\boldsymbol{p}$ to any bounded subset $\mathcal{D}$ of $\mathbb{R}^2$ required by assumption A1.

In the test SimII, the *backward* reference motion strategy has been assumed by taking $\zeta_d = -1$ (see Eq. 6). The initial robot configuration has been selected as $\boldsymbol{q}(0) = [0 \ \ -0.5 \ \ 0.5]^\top$. Results of the control process are presented by the plots in the left column in Fig. 5.

Upon the plots in Fig. 5 one can again observe fast and non-oscillatory transients of the path following errors asymptotically vanishing toward zero. A single discontinuity point seen at the very beginning of time-plot of error e_θ indicates that the auxiliary orientation angle converges in this case to θ_d only in the sense of modulo 2π (see Eq. 70). A fast convergence rate for particular errors after a first 10 s of a transient stage can be observed upon the logarithmic plot presented in Fig. 6. Again, the control signals satisfy control input limitations in the whole control time-horizon, while one can see that the VSB modifies the control inputs until about 10 s of the simulation (see the plot of $\varsigma(t)$). Also in this case, the above control performance has been obtained despite relatively large values of the initial errors, that is, for $|e_a(\boldsymbol{q}(0))| \approx 1.86$ rad and $|e_F(\boldsymbol{p}(0))| \approx 1.27$. These numbers can be confronted with the estimates determined by pairs *(p1)* and *(p2)* from Theorem 1, which in this case have been computed as follows

$$(p1): r_f = r_F = 2.8, \quad r_a \approx 1.21 \text{ rad}$$
$$(p2): r_f = \frac{r_F}{\sqrt{1+\mu\,|e_a(\boldsymbol{q}(0))|^2}} \approx 1.7, \quad r_a \approx 1.93 \text{ rad}$$

by taking $r_F = 2.8$ and $\nu = 0.9$. Note that the above values of upper bounds r_a and r_f are substantially less conservative relative to those obtained in example SimI thanks to the symmetrical shape of function (72) with respect to its zero-level curve (see Fig. 5). In this case, the initial errors satisfy conditions determined by pair *(p2)*.

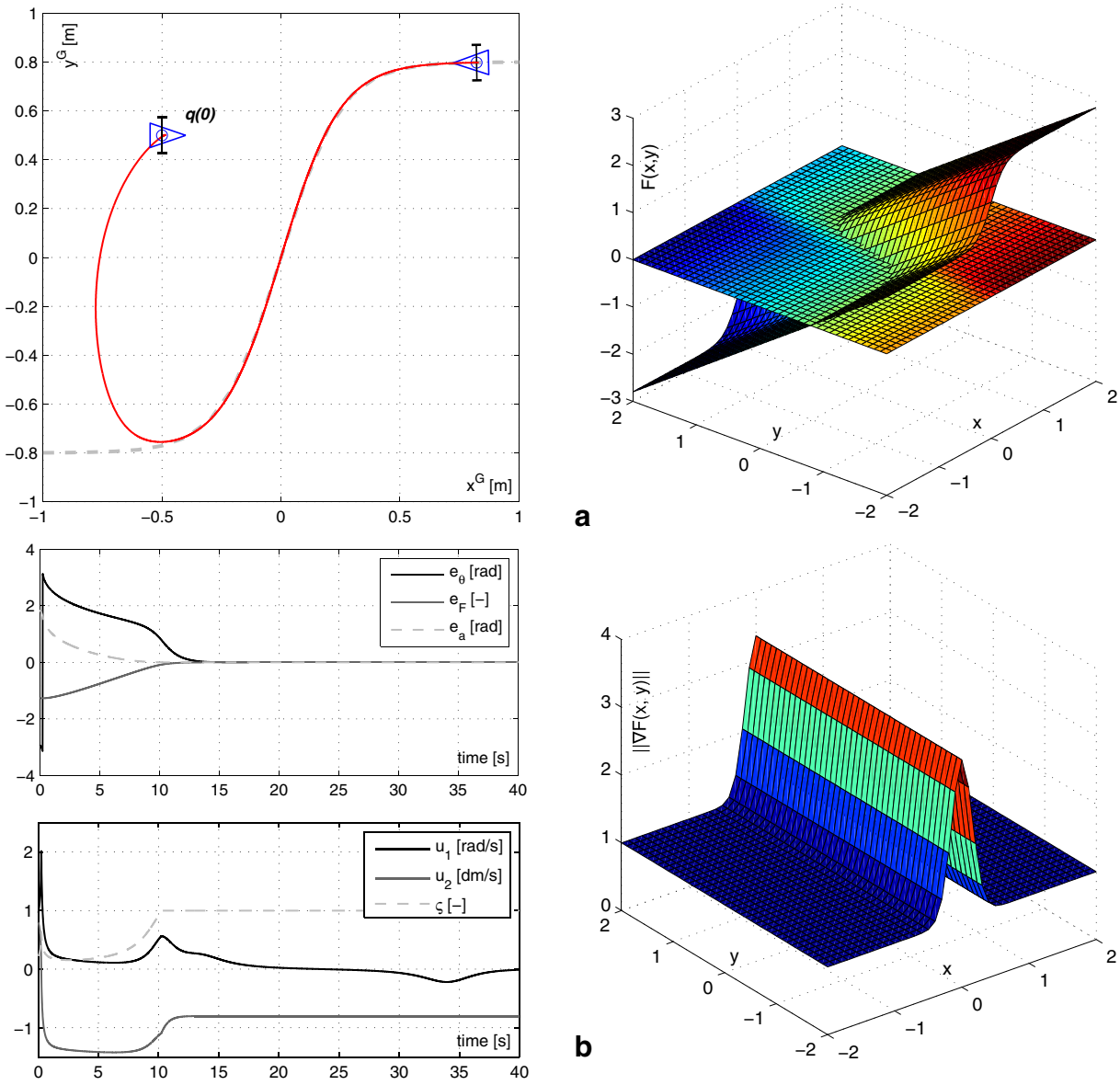

Fig. 5 SimII: control performance for the case of the S-shaped path followed in a backward motion strategy (*left column*), and the surfaces (*right column*) representing function $F(\boldsymbol{p})$, (**a**), and the norm of its gradient $\| \nabla F(\boldsymbol{p})\|$, (**b**), for argument $\boldsymbol{p} \in [-2, 2]\times[-2, 2]$

5 Experimental Verification

5.1 Description of the Experimental Setup

The proposed VFO control law has been verified experimentally on the laboratory testbed with the differentially driven mobile robot MTracker presented in Fig. 7. The robot is equipped with the on-board mini PC computer (Intel Atom processor, 2 GB of RAM), working under Linux operating system, and the DSP processor (TMS320F28335). The robot control system has a cascade structure with two independent PI velocity control loops closed around the wheel actuators and implemented on the DSP processor. The VFO control law has been implemented on the PC computer which computes the commanded wheel velocities for the inner regulation loops with sampling frequency of 100 Hz. Robust localization of the robot has been

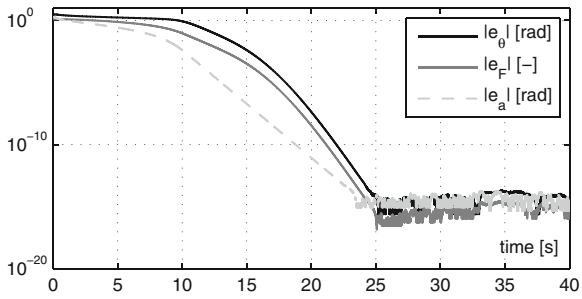

Fig. 6 SimII: absolute values of the path following errors and the auxiliary orientation error in a logarithmic scale

possible thanks to the fusion of the on-line predictor response (computed upon the kinematic model (1)) with the estimate of the robot configuration obtained from the exteroceptive Optitrack vision localization system. The block scheme shown in Fig. 7 illustrates implementation details of the control system.

5.2 Results of the Experiments

The experimental scenario has been prepared to show the control performance in the case where a reference path results from a concatenation of two zero-level curves of the fifth-degree polynomial functions joining three prescribed via points

$$\boldsymbol{q}_i = [\theta_i \; x_i \; y_i]^\top, \quad i = 0, 1, 2. \tag{73}$$

The reference path is represented by a resultant function

$$F(\boldsymbol{p}) \triangleq \begin{cases} f_1(\boldsymbol{p}) \text{ for } x \in [x_0, x_1] \\ f_2(\boldsymbol{p}) \text{ for } x \in [x_1, x_2] \end{cases} \tag{74}$$

where

$$f_i(\boldsymbol{p}) = (w_{0i} + w_{1i}x + w_{2i}x^2 + \ldots + w_{5i}x^5) - y \tag{75}$$

with particular coefficients, w_{ji}, $j = 0, \ldots, 5$, $i = 1, 2$, chosen to satisfy boundary conditions

$$\begin{aligned} & f_1(x_0, y_0) = f_2(x_2, y_2) := 0, \\ & \frac{\partial f_1}{\partial x}(x_0, y_0) := \tan\theta_0, \quad \frac{\partial f_2}{\partial x}(x_2, y_2) := \tan\theta_2, \\ & \frac{\partial^2 f_1}{\partial x^2}(x_0, y_0) = \frac{\partial^2 f_2}{\partial x^2}(x_2, y_2) := 0, \end{aligned}$$

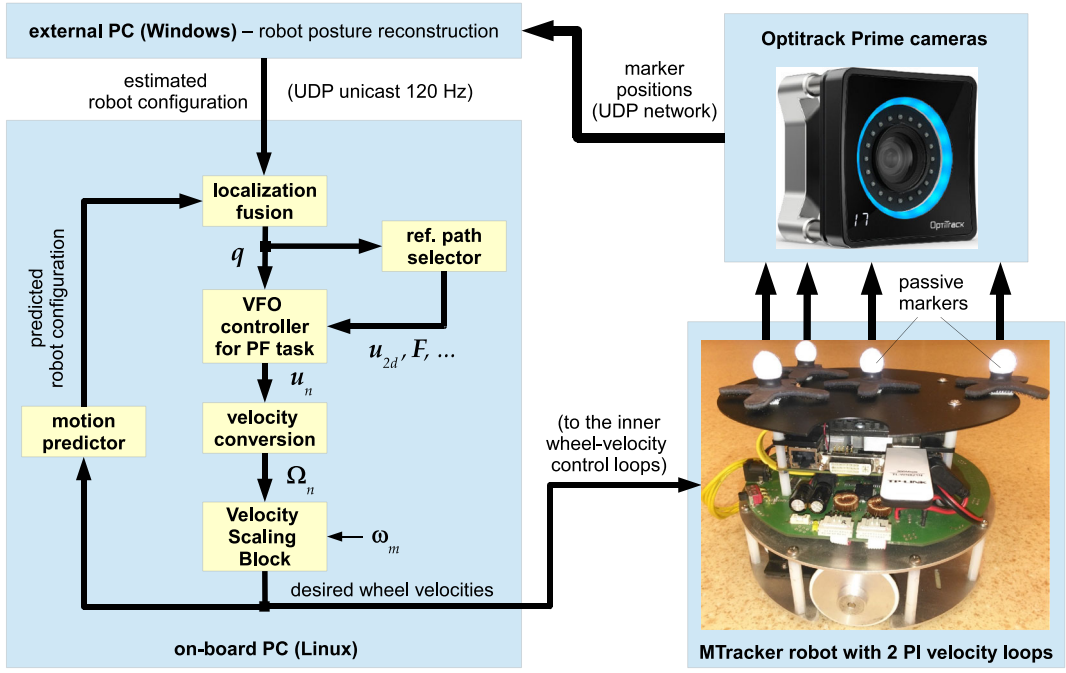

Fig. 7 A functional block scheme of the experimental setup with the MTracker mobile robot

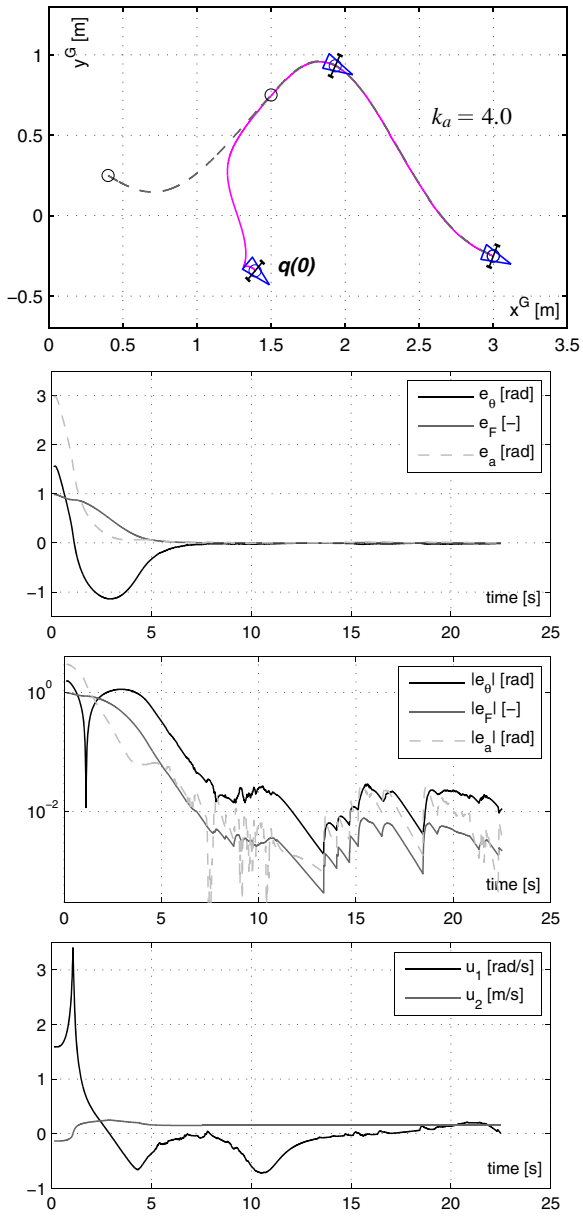

Fig. 8 Experimental results obtained for the reference path in the form of two concatenated polynomials (denoted by the *gray dashed line*) passing through three prescribed via points (denoted by the *circle marks*); initial configuration $\boldsymbol{q}(0)$ of the robot has been denoted on the X-Y plot

and three concatenation-continuity conditions at the via point $\boldsymbol{q}_1$, namely

$$
\begin{aligned}
&f_1(x_1, y_1) = f_2(x_1, y_1),\\
&\frac{\partial f_1}{\partial x}(x_1, y_1) = \frac{\partial f_2}{\partial x}(x_1, y_1) := \tan\theta_1,\\
&\frac{\partial^2 f_1}{\partial x^2}(x_1, y_1) = \frac{\partial^2 f_2}{\partial x^2}(x_1, y_1) := 0.
\end{aligned}
$$

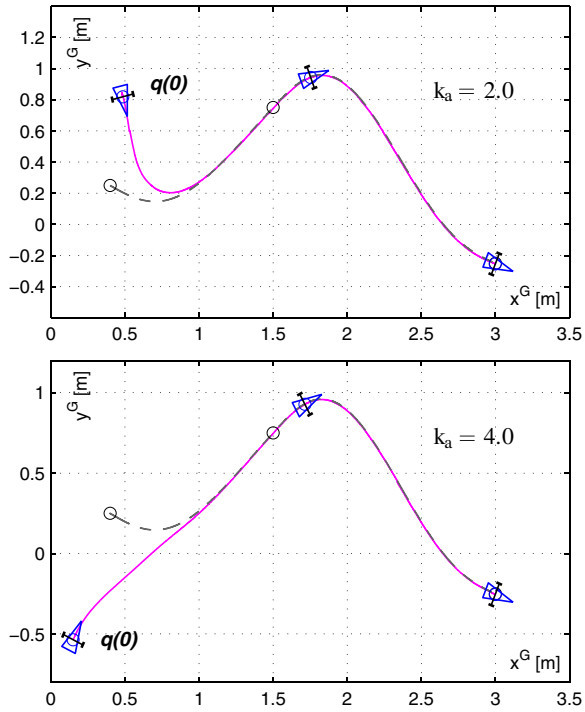

Fig. 9 Experimental results for the reference path in the form of two concatenated polynomials illustrating the control performance for two additional initial configurations $\boldsymbol{q}(0)$ of the robot

The reference path, presented in Figs. 8–9 by a dashed line, is a concatenation (74) for the following via points (denoted by the circle marks in the figures)

$$
\boldsymbol{q}_0 = \begin{bmatrix} -0.5 \\ 0.4 \\ 0.25 \end{bmatrix}, \quad \boldsymbol{q}_1 = \begin{bmatrix} 0.8 \\ 1.5 \\ 0.75 \end{bmatrix}, \quad \boldsymbol{q}_2 = \begin{bmatrix} -0.4 \\ 3.0 \\ -0.25 \end{bmatrix}.
$$

In the experiments, the following values of parameters have been used: $k_p = 1$, $k_a \in \{2, 4\}$, $v_d = 0.15\,\mathrm{m/s}$, and $\omega_m = 10\,\mathrm{rad/s}$.

Figure 8 presents the results obtained for the initial robot configuration $\boldsymbol{q}(0)$ located very far from the reference set with large initial auxiliary error $|e_a(\boldsymbol{q}(0))| \approx 2.96\,\mathrm{rad}$. Worth to emphasize the non-oscillatory and fast transient motion stage, together with boundedness of the control signals. Any substantial effect of switching from the first level curve $f_1(\boldsymbol{p}) = 0$ to the second level curve $f_2(\boldsymbol{p}) = 0$ is not visible in the plots of particular signals.

Figure 9 shows the additional results of a robot motion for two different initial configurations and two

values of the controller parameter k_a. A smooth robot motion with fast transients can be observed also in these scenarios.

Remark 7 A concatenation of splines in Eq. 74 is admissible for ranges of variable x which yield bounded partial derivatives $\partial f_i/\partial x$. If it is needed to force a motion with unbounded partial derivative with respect to x, one can cope with this problem by designing an alternative spline for this case with swapped variables x and y in Eq. 75. In general, it is also possible to concatenate two splines expressed in different ways, that is, in the form like (75) and with swapped variables.

6 Conclusions

In the paper, we have proposed and experimentally verified the novel VFO control strategy which solves the path following task for unicycle kinematics with the amplitude-limited control input. The sufficient conditions have been derived for initial errors which guarantee positionally constrained transients of the robot confined to a prescribed neighborhood of a reference path. By utilizing the level curve approach the need of a reference path parametrization has been avoided. Formal considerations provided in the paper indicate that the proposed VFO control system does not generate any additional unstable equilibria characteristic for the control system previously proposed in [26], and it concerns a wider set of reference paths than those admitted in [8].

The new solution proposed in this paper complements a set of VFO control laws available in the literature so far. As a direct consequence of the VFO methodology, the proposed control strategy inherits all the benefits characteristic for the VFO control laws like fast, non-oscillatory, and easily predictable transients in the closed loop system, and intuitive interpretation of all the control components leading to a very simple parametric synthesis of the controller. Thanks to application of the Velocity Scaling Block, which acts as a post-processing procedure of the nominal control law, one guarantees a simple solution to the path following problem in the presence of velocity constraints imposed on a robot motion.

In the paper, the VFO controller has been formulated for the generic kinematics of the unicycle. By employing the cascade control approach, application of the method can be relatively easily extended for more complex kinematics of the car-like vehicles and the non-Standard N-Trailer robots, see [22] and [20], respectively.

Acknowledgements The authors thank the anonymous reviewers for their constructive comments and suggestions which allowed improving the result presented in this paper.

Appendix A

We start by writing the equivalent form $u_2 = \varsigma\zeta_d\|\overline{\boldsymbol{h}}\|\mathrm{c}e_a$. Now, by using the following relations

$$\mathrm{c}\theta_a \overset{(18)}{=} \frac{\zeta_d h_x}{\|\overline{\boldsymbol{h}}\|}, \qquad \mathrm{s}\theta_a \overset{(18)}{=} \frac{\zeta_d h_y}{\|\overline{\boldsymbol{h}}\|}, \tag{76}$$

and upon the fact that $\mathrm{c}e_a \overset{(19)}{=} \mathrm{c}\theta_a\mathrm{c}\theta + \mathrm{s}\theta_a\mathrm{s}\theta$, one may write:

$$\begin{aligned} u_2 &= \varsigma\zeta_d\|\overline{\boldsymbol{h}}\|\mathrm{c}e_a = \varsigma\zeta_d\|\overline{\boldsymbol{h}}\|(\mathrm{c}\theta_a\mathrm{c}\theta + \mathrm{s}\theta_a\mathrm{s}\theta) \\ &= \varsigma\zeta_d\|\overline{\boldsymbol{h}}\|[\mathrm{c}\theta_a\ \mathrm{s}\theta_a]\begin{bmatrix}\mathrm{c}\theta\\ \mathrm{s}\theta\end{bmatrix} \overset{(76)}{=} \varsigma\zeta_d\|\overline{\boldsymbol{h}}\|\begin{bmatrix}\frac{\zeta_d h_x}{\|\overline{\boldsymbol{h}}\|} & \frac{\zeta_d h_y}{\|\overline{\boldsymbol{h}}\|}\end{bmatrix}\begin{bmatrix}\mathrm{c}\theta\\ \mathrm{s}\theta\end{bmatrix} \\ &= \varsigma\zeta_d^2\begin{bmatrix}h_x & h_y\end{bmatrix}\begin{bmatrix}\mathrm{c}\theta\\ \mathrm{s}\theta\end{bmatrix} = \varsigma(h_x\mathrm{c}\theta + h_y\mathrm{s}\theta) \overset{(1)}{=} \varsigma\boldsymbol{h}^\top\boldsymbol{g}_2(\theta), \end{aligned}$$

where the latter formula corresponds to the second component of control law (29).

Appendix B

The time derivative of error e_F can be expressed in the form (36) by utilizing the equivalent from of control input $u_2 \overset{(29)}{=} \varsigma(h_x\mathrm{c}\theta + h_y\mathrm{s}\theta) \equiv \varsigma\zeta_d\|\overline{\boldsymbol{h}}\|\mathrm{c}e_a$ (see Appendix A), and by using Eq. 76 together with elementary trigonometric relations:

$$\begin{aligned} \mathrm{c}\theta &\overset{(19)}{=} \mathrm{c}(\theta_a - e_a) = \mathrm{c}\theta_a\mathrm{c}e_a + \mathrm{s}\theta_a\mathrm{s}e_a, \\ \mathrm{s}\theta &\overset{(19)}{=} \mathrm{s}(\theta_a - e_a) = \mathrm{s}\theta_a\mathrm{c}e_a - \mathrm{c}\theta_a\mathrm{s}e_a. \end{aligned} \tag{77}$$

Namely,

$$\begin{aligned}
\dot{e}_F &\overset{(9)}{=} \dot{F} = F_x\dot{x} + F_y\dot{y} \overset{(1)}{=} F_x u_2 \mathrm{c}\theta + F_y u_2 \mathrm{s}\theta \\
&\overset{(29)}{=} \varsigma\,(h_x \mathrm{c}\theta + h_y \mathrm{s}\theta)(F_x \mathrm{c}\theta + F_y \mathrm{s}\theta) \\
&\equiv \varsigma\zeta_d \|\,\overline{\boldsymbol{h}}\| \mathrm{c}e_a (F_x \mathrm{c}\theta + F_y \mathrm{s}\theta) \\
&\overset{(77)}{=} \varsigma\zeta_d \|\,\overline{\boldsymbol{h}}\| \mathrm{c}e_a \,[F_x(\mathrm{c}\theta_a \mathrm{c}e_a + \mathrm{s}\theta_a \mathrm{s}e_a) \\
&\qquad + F_y(\mathrm{s}\theta_a \mathrm{c}e_a - \mathrm{c}\theta_a \mathrm{s}e_a)\big] \\
&\overset{(76)}{=} \varsigma\zeta_d \|\,\overline{\boldsymbol{h}}\| \mathrm{c}e_a \Bigg[F_x \left(\frac{\zeta_d h_x}{\|\,\overline{\boldsymbol{h}}\|} \mathrm{c}e_a + \frac{\zeta_d h_y}{\|\,\overline{\boldsymbol{h}}\|} \mathrm{s}e_a \right) \\
&\qquad + F_y \left(\frac{\zeta_d h_y}{\|\,\overline{\boldsymbol{h}}\|} \mathrm{c}e_a - \frac{\zeta_d h_x}{\|\,\overline{\boldsymbol{h}}\|} \mathrm{s}e_a \right) \Bigg] = \\
&= \varsigma \mathrm{c}e_a \left[(F_x h_x + F_y h_y)\mathrm{c}e_a + (F_x h_y - F_y h_x)\mathrm{s}e_a \right]. \quad (78)
\end{aligned}$$

Recalling definitions (16) and (17) one may write:

$$\begin{aligned}
h_x &= -v_d F_y / \|\,\nabla F\| - k_p F F_x / \|\,\nabla F\| \\
h_y &= v_d F_x / \|\,\nabla F\| - k_p F F_y / \|\,\nabla F\|.
\end{aligned}$$

Upon the above equations one can easily verify (by direct computations) that

$$(F_x h_x + F_y h_y) = -k_p F \|\nabla F\|, \quad (F_x h_y - F_y h_x) = v_d \|\nabla F\|.$$

Substituting the latter formulas to the right-hand side of Eq. 78 yields the equation of the form (36).

Appendix C

By recalling (22), (23), and (24) one may express the nominal time derivatives $\dot{h}_{xn}(\boldsymbol{q})$ and $\dot{h}_{yn}(\boldsymbol{q})$ as follows:

$$\dot{h}_{xn}(\boldsymbol{q}) = u_{2n} H_x(\boldsymbol{q}), \quad \dot{h}_{yn}(\boldsymbol{q}) = u_{2n} H_y(\boldsymbol{q}) \qquad (79)$$

where particular forms of $H_x(\boldsymbol{q})$ and $H_y(\boldsymbol{q})$ result from the combination of right-hand sides of Eqs. 23 and 24 in 22. Now, one may write

$$\begin{aligned}
\varsigma\dot{\theta}_{an}(\boldsymbol{q}) &\overset{(21)}{=} \varsigma \frac{\dot{h}_{yn}(\boldsymbol{q}) h_x(\boldsymbol{p}) - h_y(\boldsymbol{p}) \dot{h}_{xn}(\boldsymbol{q})}{h_x^2(\boldsymbol{p}) + h_y^2(\boldsymbol{p})} \\
&\overset{(79)}{=} \varsigma \frac{u_{2n} H_y(\boldsymbol{q}) h_x(\boldsymbol{p}) - h_y(\boldsymbol{p}) u_{2n} H_x(\boldsymbol{q})}{h_x^2(\boldsymbol{p}) + h_y^2(\boldsymbol{p})} \\
&\overset{(25)}{=} \frac{u_{2s} H_y(\boldsymbol{q}) h_x(\boldsymbol{p}) - h_y(\boldsymbol{p}) u_{2s} H_x(\boldsymbol{q})}{h_x^2(\boldsymbol{p}) + h_y^2(\boldsymbol{p})} \\
&\overset{(29)}{=} \frac{u_2 H_y(\boldsymbol{q}) h_x(\boldsymbol{p}) - h_y(\boldsymbol{p}) u_2 H_x(\boldsymbol{q})}{h_x^2(\boldsymbol{p}) + h_y^2(\boldsymbol{p})} \\
&= \frac{\dot{h}_y(\boldsymbol{q}) h_x(\boldsymbol{p}) - h_y(\boldsymbol{p}) \dot{h}_x(\boldsymbol{q})}{h_x^2(\boldsymbol{p}) + h_y^2(\boldsymbol{p})} \equiv \dot{\theta}_a(\boldsymbol{q}),
\end{aligned}$$

where $\dot{\theta}_a(\boldsymbol{q})$ is a time derivative of auxiliary angle (18) with time derivatives $\dot{h}_x(\boldsymbol{q})$ and $\dot{h}_y(\boldsymbol{q})$ computed by employing the scaled (admissible) control input $u_2 = \varsigma u_2^{\mathrm{VFO}}$ (in contrast to the nominal one $u_{2n} = u_2^{\mathrm{VFO}}$).

Appendix D

Computational steps of the angle $\gamma(i) = \mathrm{Atan2c}\,(z_1(i), z_2(i))$, if the arguments $z_1(i), z_2(i)$ are determined in the discrete-time domain for $i = t/T_p$ with sampling time T_p and $i \in \mathbb{N}$, can be explained as follows:

Step1 : $\Gamma(i) := \mathrm{Atan2}\,(z_1(i), z_2(i)) \in [-\pi, \pi]$

Step2 : $\Gamma(i-1) := \mathrm{Atan2}\,(\mathrm{s}\gamma(i-1), \mathrm{c}\gamma(i-1)) \in [-\pi, \pi]$

Step3 : $\Delta\Gamma(i) := \Gamma(i) - \Gamma(i-1)$

Step4 : $\Delta\gamma(i) := \Delta\Gamma(i)$

IF $\Delta\Gamma(i) > +\pi$ THEN $\Delta\gamma(i) := \Delta\Gamma(i) - 2\pi$

IF $\Delta\Gamma(i) < -\pi$ THEN $\Delta\gamma(i) := \Delta\Gamma(i) + 2\pi$

Step5 : $\gamma(i) := \gamma(i-1) + \Delta\gamma(i)$

where $\mathrm{Atan2}\,(\cdot,\cdot)$ is the four-quadrant inverse tangent function (the value range for $\mathrm{Atan2}\,(\cdot,\cdot)$ is consistent here with its implementation in Matlab).

Appendix E

Following the works [10, 11, 24, 32, 33], let us formulate an underlying definition and a theorem concerning a local version of the input-to-state stability property useful in the context of formal considerations included in Section 3.4.

Definition 2 The dynamical system

$$\dot{\boldsymbol{z}} = \boldsymbol{f}(\boldsymbol{z}, \boldsymbol{u}, t), \quad \boldsymbol{z} \in \mathcal{D}_Z, \quad \boldsymbol{u} \in \mathcal{D}_U \qquad (80)$$

with $\mathcal{D}_Z = \{\boldsymbol{z} \in \mathbb{R}^n : \|\,\boldsymbol{z}\| < r_Z\}$, $\mathcal{D}_U = \{\boldsymbol{u} \in \mathbb{R}^m : \|\,\boldsymbol{u}\| < r_U\}$ is called locally input-to-state stable (locally ISS) if there exist finite constants $r_z, r_u > 0$ and functions β of class $\mathcal{KL}$ and γ of class $\mathcal{K}$ such that for all $\boldsymbol{z}(0) \in \mathcal{D}_Z$ and $\boldsymbol{u}(t) \in \mathcal{D}_U$ satisfying $\|\,\boldsymbol{z}(0)\| < r_z$ and $\sup_{t\geq 0} \|\,\boldsymbol{u}(t)\| < r_u$ the following inequality holds

$$\|\,\boldsymbol{z}(t)\| \leq \max \left\{ \beta(\|\,\boldsymbol{z}(0)\|, t), \gamma \left(\sup_{t\geq 0} \|\,\boldsymbol{u}(t)\| \right) \right\} \qquad (81)$$

for all $t \geq 0$.

Theorem 2 *The system* (80) *is locally ISS (that is, solution* $z(t)$ *of* Eq. 80 *satisfies* (81)*) if there exists a continuously differentiable function* $V(z,t) : \mathcal{D}_Z \times [0,\infty) \to \mathbb{R}_{\geq 0}$ *and functions* $\alpha_1, \alpha_2, \alpha_3, \chi$ *of class* $\mathcal{K}$ *such that for all* $z \in \mathcal{D}_Z$, $\boldsymbol{u} \in \mathcal{D}_U$, *and* $t \geq 0$ *hold:*

$$\alpha_1(\|z\|) \leq V(z,t) \leq \alpha_2(\|z\|)$$
$$\frac{\partial V}{\partial t} + \frac{\partial V}{\partial z} \boldsymbol{f}(z,\boldsymbol{u},t) \leq -\alpha_3(\|z\|) \text{ for } \|z\| \geq \chi(\|\boldsymbol{u}\|).$$

As a consequence, the system (80) *is locally ISS according to Definition 2 with*

$$r_z = \alpha_2^{-1}(\alpha_1(r_Z)),$$
$$r_u = \chi^{-1}(\min\{r_z, \chi(r_U)\}),$$
$$\gamma(\cdot) = \alpha_1^{-1}(\alpha_2(\chi(\cdot))).$$

References

1. Bakker, T., van Asselt, K., Bontsema, J., Mller, J., van Straten, G.: A path following algorithm for mobile robots. Auton. Robot. **29**, 85–97 (2010)
2. Borhaug, E., Pavlov, A., Pettersen, K.Y.: Integral LOS control for path following of underactuated marine surface vessels in the presence of constant ocean currents. In: Proc. 47th IEEE Conf. Decision and Control, pp. 4984–4991. Cancun (2008)
3. Cheein, F.A., Scaglia, G.: Trajectory tracking controller design for unmanned vehicles: A new methodology. J. Field Robot. **31**(6), 861–887 (2014)
4. Chen, Y.-Y., Tian, Y.-P.: A curve extension design for coordinated path following control of unicycles along given convex loops. Int. J. Control **84**(10), 1729–1745 (2011)
5. Consolini, L., Maggiore, M., Nielsen, C., Tosques, M.: Path following for the PVTOL aircraft. Automatica **46**, 1284–1296 (2010)
6. Canudas, C., de Wit, B., Siciliano, Bastin, G.: Theory of Robot Control. Springer-Verlag, New York (1996)
7. DeSantis, R.M.: Path-tracking for car-like robots with single and double steering. IEEE Trans. Veh. Technol. **44**(2), 366–377 (1995)
8. Do, K.D.: Global output-feedback path-following control of unicycle-type mobile robots: A level curve approach. Robot. Autonom. Syst. **74**, 229–242 (2015)
9. Michałek, M., Kozłowski, K.: Vector-Field-Orientation feedback control method for a differentially driven vehicle. IEEE Trans. Cont. Syst. Technol. **18**(1), 45–65 (2010)
10. Isidori, A.: Nonlinear Control Systems II. Springer, London (1999)
11. Khalil, H.K. Nonlinear Systems, 3rd edn. Prentice-Hall, New Jersey (2002)
12. Klancar, G., Matko, D., Blazic, S.: Wheeled mobile robots control in a linear platoon. J. Intell. Robot. Syst. **54**, 709–731 (2009)
13. Lapierre, L., Soetanto, D., Pascoal, A.: Nonsingular path following control of a unicycle in the presence of parametric modelling uncertainties. Int. J. Robust Nonlinear Control **16**, 485–503 (2006)
14. Lapierre, L., Zapata, R.: A guaranteed obstacle avoidance guidance system. Auton. Robot. **32**, 177–187 (2012)
15. Lapierre, L., Zapata, R., Lepinay, P.: Combined path-following and obstacle avoidance control of a wheeled robot. Int. J. Robot. Res. **26**(4), 361–375 (2007)
16. Lenain, R., Thuilot, B., Cariou, C., Martinet, P.: High accuracy path tracking for vehicles in presence od sliding: Application to farm vehicle automatic guidance for agricultural tasks. Auton. Robot. **21**. 79–97 (2006)
17. Liang, Y., Jia, Y.: Combined vector field approach for 2D and 3D arbitrary twice differentiable curved path following with constrained UAVs. J. Intell. Robot. Syst. doi:10.1007/s10846-015-0308-x (2015)
18. Liu, C., McAree, O., Chen, W.-H.: Path-following control for small fixed-wing unmanned aerial vehicles under wind disturbances. Int. J. Robust. Nonlinear Control **23**, 1682–1698 (2013)
19. De Luca, A., Oriolo, G., Samson, C.: Feedback control of a nonholonomic car-like robot. In: Laumond, J.-P. (ed.) Robot Motion Planning and Control, vol. 229 LNCIS, pp. 171–253. Springer-Verlag (1998)
20. Michałek, M.: A highly scalable path-following controller for n-trailers with off-axle hitching. Control Eng. Pract. **29**, 61–73 (2014)
21. Michałek, M., Kozłowski, K.: Finite-time VFO stabilizers for the unicycle with constrained control input. In: Kozłowski, K. (ed.) Robot Motion and Control 2009, Volume 396 of Lecture Notes in Control and Information Sciences, pp. 23–34. Springer-Verlag (2009)
22. Michałek, M., Kozłowski, K.: Feedback control framework for car-like robots using the unicycle controllers. Robotica **30**(4), 517–535 (2012)
23. Michałek, M.M.: Modular tracking controller for N-trailers with non-zero hitching offsets. In: 2015 American Control Conference, pp. 5371–5376. Chicago (2015)
24. Mironchenko, A.: Local input-to-state stability: Characterizations and counterexamples. Syst. Control Lett. **87**, 23–28 (2016)
25. Morin, P., Samson, C.: Motion control of wheeled mobile robots. In: Siciliano, B., Khatib, O. (eds.) Springer Handbook of Robotics, pp. 799–826. Springer (2008)
26. Morro, A., Sgorbissa, A., Zaccaria, R.: Path following for unicycle robots with arbitrary path curvature. IEEE Trans. Robot. **27**(5), 1016–1023 (2011)
27. Płaskonka, J.: Different kinematic path following controllers for a wheeled mobile robot of (2,0) type. J. Intell. Robot. Syst. **77**, 481–498 (2015)
28. Saiki, H., Fukao, T., Urakubo, T., Kohno, T.: Hovering control of outdoor blimp robots based on path following. In: 2010 IEEE Int. Conf. Control Applications, Part of 2010 IEEE Multi-Conf. Systems and Control, pp. 2124–2129. Yokohama (2010)
29. Samson, C.: Control of chained systems. Application to path following and time-varying point-stabilization of mobile robots. IEEE Trans. Autom. Control, 64–77 (1995)

30. Sgorbissa, A., Zaccaria, R.: Integrated obstacle avoidance and path following through a feedback control law. J. Intell. Robot. Syst. **72**, 409–428 (2013)
31. Sontag, E.D.: Input-to-state stability. In: Levine, W.S. (ed.) The Control Handbook. Control system advanced methods, pp. 45-1–45-21. CRC Press (2011)
32. Sontag, E.D., Wang, Y.: New characterizations of input-to-state stability. IEEE Trans. Autom. Control **41**(9), 1283–1294 (1996)
33. Teel, A.R.: A nonlinear small gain theorem for the analysis of control systems with saturation. IEEE Trans. Autom. Control **41**(9), 1256–1270 (1996)

Maciej Marcin Michałek received the M.Sc., Ph.D., and Habilitation degrees in automation and robotics from the Poznan University of Technology (PUT), Poznań, Poland, in the years 2001, 2006, and 2015, respectively. He is currently an Assistant Professor with the Chair of Control and Systems Engineering, Faculty of Computing, PUT. His current research interests include control design problems and control applications for nonholonomic systems, in particular, for mobile robots and N-trailer vehicles, and for systems with nonminimum-phase dynamics. Dr. Michałek has been a member of the IEEE (senior member since 2016), the IEEE Robotics and Automation Society, and the IEEE Control Systems Society since 2009. He serves as an Editorial Board Member of the *Journal of Intelligent and Robotic Systems*.

Tomasz Gawron received the M.Sc. degree in automation and robotics from the Poznan University of Technology (PUT), Poznań, Poland in the year 2013. He is currently pursuing a Ph.D. degree in automation and robotics under a supervision of Dr. Maciej Marcin Michałek at the Chair of Control and Systems Engineering, Faculty of Computing, PUT. His current research is focusing on the controller-driven feedback motion planning and control of wheeled mobile robots in the presence of state and input constraints.